PONTIFICIA UNIVERSIDAD CATOLICA DE CHILE

ESCUELA DE INGENIERIA

TEMPERATURE PREDICTION IN A SOLAR POND AND THE GROUND BENEATH IT: MODEL DEVELOPMENT AND APPLICATION

JOSÉ MANUEL AMIGO ÁLVAREZ

Thesis submitted to the Office of Research and Graduate Studies in partial fulfillment of the requirements for the Degree of Master of Science in Engineering

Advisor:

FRANCISCO SUÁREZ POCH

Santiago de Chile, (April, 2017)

PONTIFICIA UNIVERSIDAD CATOLICA DE CHILE
ESCUELA DE INGENIERIA

TEMPERATURE PREDICTION IN A SOLAR POND AND THE GROUND BENEATH IT: MODEL DEVELOPMENT AND APPLICATION

JOSÉ MANUEL AMIGO ÁLVAREZ

Members of the Committee:

FRANCISCO SUÁREZ POCH

CARLOS BONILLA MELÉNDEZ

RAMÓN FREDERICK GONZÁLEZ

SERGIO GUTIÉRREZ CID

Thesis submitted to the Office of Research and Graduate Studies in partial fulfillment of the requirements for the Degree of Master of Science in Engineering

Santiago de Chile, (Abril, 2017)

A mis padres, que fueron mi mayor apoyo para culminar esta etapa.

ACKNOWLEDGEMENTS

I would first like to thank my thesis advisor, Dr. Francisco Suárez, for his time, motivation and support whenever I was having trouble with my investigation and for giving me the opportunity of presenting my work in two congresses.

I would also like to thank my family and Homero, for supporting me in every decision I made and for their affection and to my school friends from Concepción, my university companions and my sport climbing friends, for the good moments and for making this road easier.

I would also like to thank the people that helped me with experimental setup of this investigation, Andrés, José and Eduardo.

I would also like to thank the Comisión Nacional de Investigación Científica y Tecnológica (CONICYT), Chile, for funding project Fondecyt de Iniciación N°11121208, the Centro de Desarrollo Urbano Sustentable (CEDEUS – CONICYT/FONDAP/15110020), and the Center for Solar Energy Technologies (CSET—CORFO CEI2-21803), which supported this investigation

CONTENTS

Page

LIST OF TABLES

Page

LIST OF FIGURES

Page

RESUMEN

Las pozas solares son colectores solares de bajo costo que pueden almacenar calor en el largo plazo y entregar calor tanto en el día como en la noche. Estas pozas consisten en cuerpos de agua artificialmente estratificados que almacenan el calor en el fondo de ellas. Dado a que las mayores temperaturas se alcanzan en el fondo, parte del calor almacenado puede perderse hacia el suelo, afectando así su eficiencia. Es por ello, que por motivos de diseño u operación, es relevante poder tener una buena representación de los flujos de calor en el lecho de una poza solar. En este estudio, un modelo unidimensional transiente se desarrolla para representar la evolución térmica de una poza solar y el suelo bajo ésta. El método implícito de diferencias finitas es utilizado para resolver las ecuaciones de conservación. El modelo es calibrado y validado con una poza solar experimental y tres pozas solares adicionales de literatura, ubicadas en El Paso, Kuwait City y Barcelona. Además, para estudiar el efecto del almacenamiento de calor en el suelo sobre el desempeño de una poza solar, dos escenarios hipotéticos son modelados: uno con una capa de aislante bajo la poza y otro sin, y en ambos escenarios se extrae calor a una tasa constante desde el fondo de las pozas. Los resultados demuestran que cuando no se usa aislante, el suelo bajo la poza actúa como un volumen de almacenamiento de calor adicional, permitiendo temperaturas más estables a lo largo del año y recuperando hasta un 25.5% del calor que se almacena en el suelo durante los meses de invierno. Un análisis de sensibilidad demuestra que la temperatura del fondo de la poza tiene una relación lineal con la conductividad térmica del suelo y una relación logarítmica con la profundidad de la napa freática.

ABSTRACT

Salt-gradient solar ponds are long-term low-cost solar collectors that can store low-grade heat and can deliver it continuously during day and night. These ponds are artificially stratified water bodies that store the heat at its bottom. As the highest temperatures in the pond are achieved at the bottom, part of the stored heat is lost to the ground, affecting the pond's efficiency. Therefore, for design or operation purposes is relevant to have a good representation of the energy fluxes at the pond's bottom boundary and the ground beneath it. In the present study, a one-dimensional transient model is developed to represent the thermal evolution of a salt-gradient solar pond and the ground that surrounds it. The implicit finite difference method is used for solving the conservation equations. The model is calibrated and validated with an experimental SGSP and three additional literature SGSPs, located in El-Paso, Kuwait City and Barcelona. Further, to study the effect of the ground heat storage over the pond's performance, two hypothetical scenarios were modeled with a constant heat removal from the LCZ, the first with an insulation layer beneath the pond and the second without it. Results show that when no insulation is used, the ground below the pond acts as an additional heat storage volume, permitting more stable temperatures through the year and recovering 25.5% of the heat that was stored in the ground during the winter period. A sensitivity analysis showed that the pond's temperature has a linear relation with the ground's thermal conductivity and a logarithmic relation with the water table depth.

1 INTRODUCTION

The increasing energy demand together with international requirements for greenhouse gas emission reduction, have given space for developing sustainable technologies (Valderrama et al., 2011). Solar, wind, hydro and geothermal energies are some examples of the most promising eco-friendly energy sources (Panwar et al., 2011). Solar energy is probably the most desirable energy source as it is the most abundant (~1.8×10^{14} kW are intercepted by the Earth) and it is not exhaustible (Kannan and Vakeesan, 2016). Nevertheless, it has two main disadvantages: (i) due to its diffusive nature, it requires large area collectors to capture a significant amount of energy, which results in high investment costs; (ii) it is an intermittent energy resource as it is only available during part of the day, so heat must be stored to have a continuous supply in time (Kannan and Vakeesan, 2016; Singh et al., 1994). Salt-gradient solar ponds (SGSPs) are low-cost solar collectors that can store heat from the solar radiation in the long-term and can deliver it during the day and night (Prasad and Rao, 1993; Rabl and Nielsen, 1975; Ruskowitz et al., 2014). Even though SGSPs are less efficient than photovoltaic collectors, it has been proven that SGSPs have a lower cost/efficiency ratio (Hull et al., 1989). In sites with high levels of solar radiation and availability of land and brine at a low cost, SGSPs can be a promising technology for heat collection and storage (Bronicki, 2013). Heat extraction is the main aim in the design of SGSPs (Jaefarzadeh, 2006) and it can be used for multiple applications like heating of buildings (El-Sebaii et al., 2011; Styris and Harling, 1976), power production (El-Sebaii et al., 2011; Singh et al., 2011), industrial process heating (El-Sebaii et al., 2011; Garrido et al., 2012) and desalination (El-Sebaii et al., 2011; Suárez et al., 2010a; Suárez et al., 2015; Suárez and Urtubia, 2016).

An SGSP is a water body with three typical regions: the upper convective zone (UCZ), the non-convective zone (NCZ) and the lower convective zone (LCZ) (Kurt et al., 2000), as shown in Figure 1-1. The LCZ consists in a homogeneous solution with high concentrations of salts. Above it, in the NCZ, a salinity gradient is established such that water closer to the surface is always less salty than the water below it. This region acts as an insulating layer of the LCZ, because as the hotter saltier water at the bottom of the gradient remains denser than the colder less salty water above it, no convection occurs (Saleh et al., 2011). Therefore, the only heat loss from the LCZ to the UCZ is due to conduction. If the NCZ is thick enough and as the water's thermal conductivity is relatively low, the conductive heat flux is small and allows achieving high temperatures at the bottom (Lu et al., 2001) with typical temperatures ranging between 50 and 90°C (Busquets et al., 2012). Lastly, the UCZ is formed by a thin layer of fresh water and its main purpose is to protect the salt gradient from wind and evaporation (Hull et al., 1989).

The development of computational tools that allow simulation of SGSP thermal behavior is important for better design and performance evaluation of these systems. Further, given that heat losses to the ground beneath the SGSP play an important role in the pond's efficiency, multiple models have included the ground in the numerical analysis (Bernad et al., 2013; Sezai and Tasderimoglu, 1995; Date et al., 2013; Wang and Akbarzadeh, 1982; Sayer et al., 2016; Tundee et al., 2010; Zhang and Wang, 1990; Kurt et al., 2006; Ali, 1986). Nevertheless, none of these models have described the temperature distribution in the ground beneath a SGSP and been validated simultaneously.

The general objective of this investigation is to study the impact of the ground heat storage capacity on the performance of an SGSP. The specific objectives are: 1) to develop a one-dimensional transient model for predicting the temperatures in an SGSP and the ground beneath it; 2) to calibrate and validate the model with experimental and literature data; 3) to simulate two hypothetical SGSPs with heat removal from the LCZ: one with an insulation layer beneath it and the other without an insulation layer and study the effect of having ground heat storage in the operation of them; 4) to study the most influent variable in the ground heat storage under a SGSP.

This thesis is structured in two chapters. The first chapter, corresponds to a manuscript called "A transient model for temperature prediction in a salt-gradient solar pond and the ground beneath it", where the specific objectives 1 and 2 are accomplished. The second chapter corresponds to a manuscript called “The role of ground heat storage capacity on the operation of a solar pond”, where the specific objectives 3 and 4 are accomplished. Both manuscripts will be submitted for peer-review.

2 A TRANSIENT MODEL FOR TEMPERATURE PREDICTION IN A SALT-GRADIENT SOLAR POND AND THE GROUND BENEATH IT

2.1 Abstract

Salt-gradient solar ponds are long-term low-cost solar collectors that can store low-grade heat and can deliver it continuously during day and night. These ponds are artificially stratified water bodies that store the heat at its bottom. As the highest temperatures in the pond are achieved at the bottom, part of the stored heat is lost to the ground, affecting the pond's efficiency. Therefore, for design or operation purposes is relevant to have a good representation of the energy fluxes at the pond's bottom boundary and the ground beneath it that can be used to develop computational tools that allow the simulation of the thermal behavior of these water bodies. In the present study, a one-dimensional transient model is developed to represent the thermal evolution of a salt-gradient solar pond and the ground that surrounds it. The implicit finite difference method is used for solving the conservation equations. Experimental data from an indoor laboratory-scale solar pond is used for the development, calibration and validation of the model. Further, the model is validated with information from three outdoor salt-gradient solar ponds available in literature located in El Paso, Kuwait City and Barcelona.

Keywords: solar pond, transient model, solar energy

2.2 Nomenclature

k	thermal conductivity [W/m/K]	T	temperature [°C]
C_P	specific heat [kJ/kg/K]	z	depth [m]
s	salinity [% kg/kg]	w	portion of radiation lost in the air [-]
Q_c	conductive heat flux [W/m^2]	I	shortwave radiation [W/m^2]
Q_g	convective heat flux lost to the ground [W/m^2]	I_0	incident radiation at the solar pond's surface [W/m^2]
Q_w	convective heat flux lost to the walls [W/m^2]	h_1	convective heat coefficient between the bottom of the solar pond and the ground beneath [W/m^2/°C]
U_2	wind speed at 2 meters from the solar pond's surface	h_2	convective heat coefficient between the ground and the groundwater sink [W/m^2/°C]
Δt	time step length [s]	U_w	overall convective heat transfer coefficient between the perimeter of the pond and the position of a known temperature
Δz	layer thickness [m]	Q_{free}	free convection heat flux [W/m^2]
Q_{forced}	forced convection heat flux [W/m^2]	Q_l	total long-wave radiation heat flux [W/m^2]
Q_{lw}	long-wave radiation from the solar pond to the atmosphere [W/m^2]	Q_{la}	long-wave radiation from the air to the solar pond [W/m^2]
Q_s	sensible heat flux [W/m^2]	Q_e	evaporative heat flux [W/m^2]
Q_{use}	extracted heat [W/m^2]	h	altitude [m]
R	equivalent thermal resistance [m^{2}K/W]	x_g	distance between the solar pond perimeter and the position of a known temperature[m]
e_{sw}	saturated vapor pressure on the water surface [Pa]	e_{sat}	saturated vapor pressure in the air [Pa]
e_a	vapor pressure in the air [Pa]	P_{atm}	pressure [Pa]
T_{av}	virtual temperature of air [°C]	T_{wv}	virtual temperature of water [°C]

Greek Symbols

ρ	density [kg/m^3]	η	extinction coefficient [-]
α	albedo [-]	β	portion of radiation lost in the air [-]
μ	absorption coefficient [-]	ϵ	emissivity [-]
σ	Stephan-Boltzmann coefficient [W/m^2/°C]		

Subscripts/superscripts

i	layer number in the SGSP	gw	groundwater
k	layer number in the ground	$SGSP$	salt-gradient solar pond
n	time step	w	fresh water
U	upper convective zone	obs	experimental
L	lower convective zone	sim	modeled
N	deepest layer	g	ground
a	air	ds	dry sand
ms	moist sand	c	concrete

2.3 Introduction

The increasing energy demand together with international requirements for greenhouse gas emission reduction, have given space for developing sustainable technologies (Valderrama et al., 2011). Solar, wind, hydro and geothermal energies are some examples of the most promising eco-friendly energy sources (Panwar et al., 2011). Solar energy is probably the most desirable energy source as it is the most abundant (~1.8×10^{14} kW are intercepted by the Earth) and it is not exhaustible (Kannan and Vakeesan, 2016). Nevertheless, it has two main disadvantages: (i) due to its diffusive nature, it requires large area collectors to capture a significant amount of energy, which results in high investment costs; (ii) it is an intermittent energy resource as it is only available during part of the day, so heat must be stored to have a continuous supply in time (Kannan and Vakeesan, 2016; Singh et al., 1994). Salt-gradient solar ponds (SGSPs) are low-cost solar collectors that can store heat from the solar radiation in the long-term and can deliver it during the day and night (Prasad and Rao, 1993; Rabl and Nielsen, 1975; Ruskowitz et al., 2014). Even though SGSPs are less efficient than photovoltaic collectors, it has been proven that SGSPs have a lower cost/efficiency ratio (Hull et al., 1989). In sites with high levels of solar radiation and availability of land and brine at a low cost, SGSPs can be a promising technology for heat collection and storage (Bronicki, 2013). Heat extraction is the main aim in the design of SGSPs (Jaefarzadeh, 2006) and it can be used for multiple applications like heating of buildings (El-Sebaii et al., 2011; Styris and Harling, 1976), power production (El-Sebaii et al., 2011; Singh et al., 2011), industrial process heating (El-Sebaii et al., 2011; Garrido et al., 2012) and desalination (El-Sebaii et al., 2011; Suárez et al., 2010a; Suárez et al., 2015; Suárez and Urtubia, 2016).

An SGSP is a water body with three typical regions: the upper convective zone (UCZ), the non-convective zone (NCZ) and the lower convective zone (LCZ) (Kurt et al., 2000), as shown in Figure 1-1. The LCZ consists in a homogeneous solution with high concentrations of salts. Above it, in the NCZ, a salinity gradient is established such that water closer to the surface is always less salty than the water below it. This region acts as an insulating layer of the LCZ, because as the hotter saltier water at the bottom of the gradient remains denser than the colder less salty water above it, no convection occurs (Saleh et al., 2011). Therefore, the only heat loss from the LCZ to the UCZ is due to conduction. If the NCZ is thick enough and as the water's thermal conductivity is relatively low, the conductive heat flux is small and allows achieving high temperatures at the bottom (Lu et al., 2001) with typical temperatures ranging between 50 and 90°C (Busquets et al., 2012). Lastly, the UCZ is formed by a thin layer of fresh water and its main purpose is to protect the salt gradient from wind and evaporation (Hull et al., 1989).

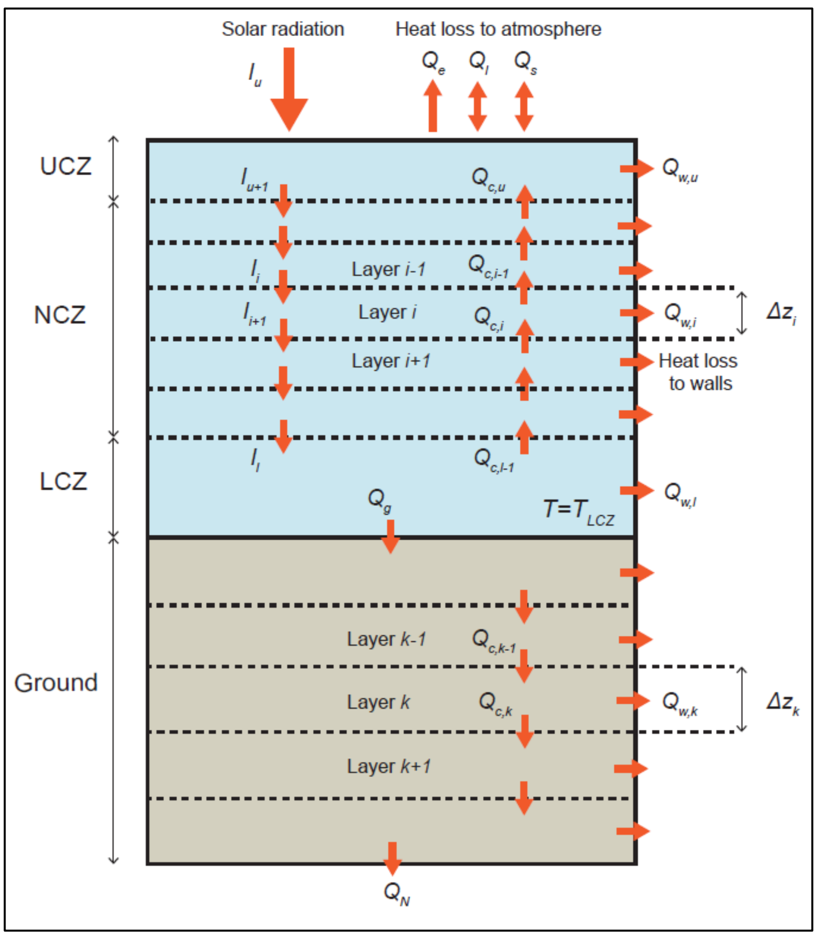

Figure 2-1: Characteristic regions in an SGSP and heat fluxes governing its thermal dynamics.

The development of computational tools that allow simulation of SGSP thermal behavior is important for better design and performance evaluation of these systems. Several analytical (Rabl and Nielsen, 1975; Weinberger, 1964; Hawas and Elasfouri, 1985) and numerical models (Singh et al., 1994; Prasad and Rao, 1995; Bernad et al., 2013; Sezai and Tasderimoglu, 1995; Date et al., 2013; Wang and Akbarzadeh, 1982; Sayer et al., 2016; Tundee et al., 2010; Zhang and Wang, 1990; Kurt et al., 2006; Ali, 1986; Suárez et al., 2010b; Hilgerson et al. (under review)) have been proposed to describe and predict the temperature distribution in SGSPs. Although analytical models are less expensive to construct and may be a good approximation for steady state regime, they fail when unsteady conditions need to be studied (Wang and Akbarzadeh, 1990). For example, analytical models generally assume that the air temperature and the solar radiation can be represented as sinusoidal functions with yearly periods, which may not always represent the reality. Also, the brine's thermal properties, considered constant in analytical models, are dependent on temperature and salinity, and may have significant variations when these variables change. Numerical models instead, can be adapted to specific and transient scenarios. The most common approach of numerical models is to treat the NCZ of the SGSP as a one-dimensional unsteady conduction later with internal heat generation due to radiation absorption, and the UCZ and LCZ as completely mixed zones. Typically, the conservation equations are solved using the finite difference method (Date et al., 2013; Wang and Akbarzadeh, 1990). Further, as heat losses to the ground beneath the SGSP play an important role in the pond's efficiency, multiple models have included the ground in the numerical analysis (Bernad et al., 2013; Sezai and Tasderimoglu, 1995; Date et al., 2013; Wang and Akbarzadeh, 1982; Sayer et al., 2016; Tundee et al., 2010; Zhang and Wang, 1990; Kurt et al., 2006; Ali, 1986). Tundee et al. (2010) and Sayer et al. (2013) built numerical models in which the ground beneath the SGSP was treated as a single layer that separated the SGSP from the groundwater table. In their work, heat losses were estimated using a convective heat transfer coefficient to represent the overall ground's thermal resistance. Even though the models were validated with experimental data, they did not describe the temperature distribution in the ground, and only a constant gradient of temperature could be assumed between the SGSP's bottom and the groundwater table, which can be unrealistic under certain conditions. According to Zhang and Wang (1990), when heat is removed from the SGSP during cold periods, the ground acts as an additional heat storage volume. Given that the SGSP is cooled when heat is extracted, the ground beneath the pond has a higher temperature than the LCZ and heat flows into the pond enhancing heat storage (Zhang and Wang, 1990). This scenario, for example, cannot be correctly represented when a single layer is used to describe the complete domain of the ground, but the subdivision of the ground in multiple layers could. Date et al. (2013) and Wang and Akbarzadeh (1982) instead, developed numerical models in which the ground was divided in more layers, but their models did not consider the groundwater table depth. Thus, their models were limited to specific scenarios in which the groundwater table is deep enough so heat losses towards the groundwater were not considerable. Zhang and Wang (1990) developed a similar model than that of Date et al. (2013), but in this case the depth to the groundwater table was included. Nevertheless, all of these models were not validated with experimental data (Date et al., 2013; Wang and Akbarzadeh, 1982; Zhang and Wang, 1990). Furthermore, one of the unresolved issues in SGSP modelling is that most of the numerical models developed so far do not consider the conductive heat losses to the ground through the pond's perimeter. All the models reviewed assume that these heat losses are negligible in order to simplify the numerical analysis. This simplification may be realistic for large-scale SGSP's but may be unrealistic for small-scale ponds. In any case, if the edge effects are considered, the ground heat losses should mildly increase as typically the perimeter of the pond will be cooler than the pond itself (Hull et al., 1989).

In the present study, a one-dimensional transient model was developed to represent the thermal evolution of an SGSP and the ground that surrounds it. The ground under the pond was discretized into multiple layers and perimeter heat losses were considered. The model was calibrated and validated using an indoor laboratory-scale solar pond, where artificial lights were used to mimic the solar radiation. Further, the model was validated with data from three SGSPs available in literature (Lu et al., 2009; Valderrama et al., 2011; Ali, 1986), all exposed to atmospheric conditions. The aim of this work is to build a simple and flexible tool for predicting temperatures in an SGSP and the ground beneath it, capable of representing multiple scenarios, with the feature of including detailed ground heat fluxes.

2.4 Materials and methods

2.4.1 Mathematical model

The thermal evolution in an SGSP can be treated as a one-dimensional transient conduction problem with internal heat generation (Lu et al., 2009). The implicit finite-difference method can be used to describe the thermal dynamics in the SGSP and the ground beneath it. Because of that, the domain is divided into multiple horizontal layers, each of them with uniform properties (Figure 1). On one hand, our model assumes that the UCZ and the LCZ are convective zones, i.e., their temperatures are uniform and therefore, they are treated as single layers. On the other hand, multiple thinner layers are used to represent the NCZ and the ground beneath the SGSP. The salt diffusion process is not considered in the model, thus the thicknesses of the different regions in the SGSP (UCZ, NCZ and LCZ) are assumed to be fixed in time. This assumption was made because of the much larger temporal scale of salt diffusion compared to thermal diffusion (Hull et al. 1989). Salt water properties are defined according to equations (1.1), (1.2) and (1.3) (Kauffmann, 1960). The density of fresh water ρ_w is assumed to be 1,000 kg m^{-3}, as in standard conditions (Hawas and Elasfouri, 1985).

$$k_i = 0.5553 - 0.0000813\left(\frac{s_i}{100}\rho_w\right) + 0.0008(T_i^n - 20) \tag{1.1}$$

$$\rho_i = 998 - 0.65\left(\frac{s_i}{100}\rho_w\right) + 0.4(T_i^n - 20) \tag{1.2}$$

$$C_{P,i} = 4{,}180 - 4.396\left(\frac{s_i}{100}\rho_w\right) + 0.0048\left(\frac{s_i}{100}\rho_w\right)^2 \tag{1.3}$$

The energy balance in the NCZ is governed by the heat diffusion Q_c, with two additional fluxes corresponding to the heat losses to the walls that surround the pond Q_w and the energy source associated to the radiative flux I (Sezai and Tasdemiroglu, 1995). The NCZ thermal evolution is described by:

$$\rho_i^n C_{P,i}^n \Delta z_i \left(\frac{T_i^{n+1} - T_i^n}{\Delta t} \right) = Q_{c,i}^{\mathrm{n+1}} + Q_{c,i-1}^{\mathrm{n+1}} + I_i - Q_{w,i} - I_{i+1} \tag{1.4}$$

The attenuation of the radiation through the water column is assumed to be exponential and it is calculated with two different expressions depending on whether the radiative fluxes come from artificial lights or natural sunlight, as shown in equation (1.5). When the radiative fluxes come from artificial lights, the attenuation is described by the Beer's law (Kurt et al., 2006). The albedo (α) represents the fraction of incident radiation that is reflected to the atmosphere and it is assumed to be 0.08, based on the usual adopted values in previous studies (Kurt et al., 2000; Kurt et al., 2006). The absorption coefficient (β) represents the fraction of longwave radiation that is absorbed in the first millimeters of water. The extinction coefficient (η) describes the attenuation of the shortwave radiation through the water column. Both β and η are dependent of the range of the wavelength spectrum, but as no measurements or detail information was available for the experimental setup, these parameters were calibrated. Further, an additional parameter w is used to represent the fraction of radiation lost in the air between the SGSP's surface and the elevation at which radiation is measured, that is only significant in experimental SGSPs. For instance, in previous experiments where high intensity discharge lamps were used, a 38.5% of solar radiation attenuation was measured in 10 cm of air (Ruskowitz et al., 2014; Suárez et al., 2011; Suárez et al., 2014a). When the radiative fluxes come from solar radiation instead, the attenuation can be better described by the Rabl and Nielsen expression, as it uses specific absorption and extinction coefficient for the different ranges of wavelength in the solar spectrum (Rabl and Nielsen, 1975).

$$I(z) = \begin{cases} (1-w)(1-\alpha)(1-\beta)I_0 \exp(-\eta z) & ,for\ artificial\ lights \\ (1-\alpha)I_0 \sum_{j=1}^{4} (1-\beta_j) \exp(-\eta_j z) & ,for\ solar\ radiation \end{cases} \tag{1.5}$$

with	for wavelengths
β_1=0.00032, η_1=0.237m^{-1}	0.2-0.6 µm
β_2=0.0045; η_2=0.193 m^{-1}	0.6-0.75 µm
β_3=0.03; η_3=0.167 m^{-1}	0.75-0.9 µm
β_4=0.35; η_4=0.179 m^{-1}	0.9-1.2 µm

Heat conduction from the i^{th} layer to the layer beneath is calculated using a discretized form of Fourier's Law:

$$Q_{c,i}^{n+1} = \left(\frac{k_i + k_{i+1}}{2}\right)\left(\frac{T_i^{n+1} - T_{i+1}^{n+1}}{\Delta z_i}\right) \tag{1.6}$$

Heat losses to the sidewalls, $Q_{w,i}$, are estimated as convective fluxes with the following equation:

$$Q_{w,i} = U_w(T_i^{n+1} - T_a^{n+1}) \tag{1.7}$$

where U_w is the overall convective heat coefficient between the perimeter and the boundary in which the temperature (T_a) is known.

The energy balance for the UCZ is given by equation (1.8).The heat fluxes at the SGSP water surface are given by evaporation losses, net long-wave radiation and the sensible heat. Details of the calculation of these heat fluxes can be found in Appendix A.

$$\rho_U^n C_{P,\mathrm{U}}^n z_U \left(\frac{T_U^{n+1} - T_U^n}{\Delta t}\right) = Q_{C,U}^{\mathrm{n+1}} + I_U - I_{U+1} - Q_e - Q_l - Q_s - Q_{w,\mathrm{u}} \tag{1.8}$$

The energy balance for the LCZ is given by:

$$\rho_L C_{P,\mathrm{L}} z_L \left(\frac{T_L^{n+1} - T_L^n}{\Delta t}\right) = Q_{C,L-1} + I_L - Q_{w,\mathrm{L}} - Q_g - Q_{use} \tag{1.9}$$

where Q_{use} is the extracted heat from the LCZ and Q_g is the convective heat loss to the ground, which is calculated as:

$$Q_g = h_1 (T_{L+1}^{n+1} - T_L^{n+1}) \tag{1.10}$$

The convective heat coefficient between the LCZ and the bottom of the SGSP, h_1, is assumed to be constant and equal to 78.12 W m^{-2} K^{-1} (Sodha et al., 1980).

Finally, the energy balance for the k^{th} layer in the ground beneath the pond is given by:

$$\rho_k C_{P,k} \Delta z_k \left(\frac{T_k^{n+1} - T_k^n}{\Delta t}\right) = Q_{\mathrm{c,k}} + Q_{\mathrm{c,k-1}} + Q_{w,k} \tag{1.11}$$

2.4.2 Boundary conditions

The mathematical model requires upper, lower and lateral boundary conditions. Meteorological data, i.e., radiation, relative humidity, air temperature and wind speed are typically measured in the ambient surrounding an SGSP and are used to calculate the heat fluxes that are used as upper boundary conditions (see Appendix A). The lower boundary of the model is described by a known energy flux at the N^{th} layer of the domain, Q_N, which is calculated with equation (1.12) This energy flux can represent the interaction between the ground and the groundwater table or the temperature at some specific depth in the ground (i.e., when the groundwater table is located very deep). If the domain limits with ground at its bottom, the heat flux is given by conduction and described by Fourier’s Law. When the bottom of the domain limits with the phreatic level instead, Q_N is estimated as a convective heat flux, where h_2 (= 185.8 W m^{-2} K (Sodha et al., 1980)) represents the convective heat coefficient between the ground and the groundwater, which acts as a sink.

$$Q_N^{n+1} = \begin{cases} K_N \dfrac{\left(T_g^n - T_N^n\right)}{\Delta z_N} & ,if\ lower\ boundary\ limits\ with\ ground \\ h_2(T_w^n - T_N^n) & ,if\ lower\ boundary\ limits\ with\ the\ groundwater\ table \end{cases} \tag{1.12}$$

A known lateral energy flux, Q_w, from the SGSP's perimeter is used as the lateral boundary condition and calculated with equation (1.13). For unburied ponds, Q_w represents the lateral heat losses from the SGSP to the air surrounding the SGSP. For buried SGSPs instead, Q_w represents a convective flux between the SGSP's perimeter and a certain lateral distance x_g, where heat fluxes coming from the pond are negligible and the temperature in the ground can be assumed constant and equal to the yearly average of the ambient (T_{avg}) (Date et al., 2013).

$$Q_{w,i}^{n+1} = \begin{cases} U_{w,i}(T_a^n - T_i^n) & ,for\ unburied\ SGSPs \\ U_{w,i}\left(T_{avg}^n - T_i^n\right) & ,for\ buried\ SGSPs \end{cases} \tag{1.13}$$

For both scenarios, the overall convective heat coefficient (U_w) is estimated as the inverse sum of the resistances to heat transfer between the SGSP and the boundary in which the temperature is known, according to equation (1.14). The subindex m represents different materials (e.g., concrete wall, sand surrounding the wall), M is the total number of materials, and R_m the equivalent thermal resistance to heat transfer due to conduction.

$$U_{w,i} = \frac{1}{\sum_{m=1}^{M} R_{m,i}} = \frac{1}{\sum_{m=1}^{M} \frac{x_m}{k_m}} \tag{1.14}$$

2.4.3 Experimental setup

The development and calibration of the model were performed using a small-scale experimental SGSP. The pond was rectangular in shape with vertical sidewalls, a 2.82-m^2 surface and a depth of 0.93 m. An 11-cm thickness layer of concrete surrounded the SGSP. The bottom and the walls of the SGSP were painted black to minimize the reflected radiation and to maximize radiation absorption. The pond was constructed inside a tank filled with sand, as shown in Figure 1-2(a). The pond was constructed indoor, in order to have controlled environmental conditions (Figure 1-2(b)). Six high-intensity discharge lamps (Virtual Sun VSD1000WDS 1000W Dimmable MH/HPS Digital Grow) were used to mimic solar radiation, with the light covering a spectrum ranging between 350 and 770 nm. The amount of incident radiation during the daily cycle was regulated through the lamps power (750, 1,000 or 1,100 W), and turning on and off the lights using a timer that was programmed according to the desired operating conditions.

Short-wave radiation was measured 7 cm above the SGSP's surface using a pyranometer (LP02, Hukseflux) and data were collected in a CR10 datalogger (Campbell Sci., Logan, UT). Temperatures of the air, the water column and the ground beneath the SGSP were measured with a vertical high-resolution distributed temperature sensing (DTS) system similar to that presented by Suárez et al. (2011), with a temperature precision of ±0.01°C when 5-min integration intervals were chosen. The cable was installed around a plastic tube and temperatures were measured every 1.1 cm depth within the water column and the ground beneath it (Figure 1-2(a)). Relative humidity was measured 8 cm above the SGSP's surface using a digital humidity sensor (SHT1X, Sensirion, Switzerland) and data was collected in a microcontroller (Arduino UNO R3). All the instrumentation used in the experiment recorded data every 5 minutes.

The salt gradient establishment and the SGSP filling were done as described by Ruskowitz et al. (2014). The LCZ was filled until a 39-cm height with a saturated sodium chloride solution (~26%w). The NCZ was created by consecutively adding 26 layers of decreasing salinity solutions of ~1.7 cm thickness. Each solution was previously prepared by diluting saturated sodium chloride solutions to the desired concentration, and was pumped onto a plastic diffuser that floated on the water's surface (Figure 1-2(c)). To have a minimum impact on the salt gradient, the saline solution was released slowly to the SGSP through the small holes at the bottom of the floating diffuser. At last, a 10-cm layer of fresh water was poured on top of the SGSP to form the UCZ. An 8-cm diameter salt-charger was installed next to one of the SGSP's wall to maintain a saturated concentration in the bottom (Figure 1-2(b)). The salt charger opening's heights defined the position of the NCZ-LCZ interface and fixed the LCZ thickness. Further, fresh water was pumped at a constant rate of 1 L/h from a 60-L tank, into the UCZ through an inlet pipe located at 90 cm from the bottom of the SGSP. On the opposite side of the SGSP, an outlet pipe installed at 93 cm from the bottom returns the water to the tank, maintaining the SGSP depth fixed. Due the water lost by evaporation, the tank had to be refilled with fresh water to have a constant supply in time. The amount of water loss by evaporation was monitored as the tank was permanently on a balance (Midrics 1, Sartorious, Germany), and the weight was measured every 10 s, with a precision of ±0.005 kg (Figure 1-2(d)).

Despite the SGSP's depth and LCZ thickness were maintained constant in time, the UCZ and NCZ thicknesses and concentrations varied during the experiments. As salt diffuses from higher to lower concentrations, the UCZ's concentration increased with time, implying that the upper layers of the NCZ mixed with the UCZ. Because of this, the UCZ thickness increased with time and the NCZ thickness decreased. The SGSP's operation began on May 18th, 2015.

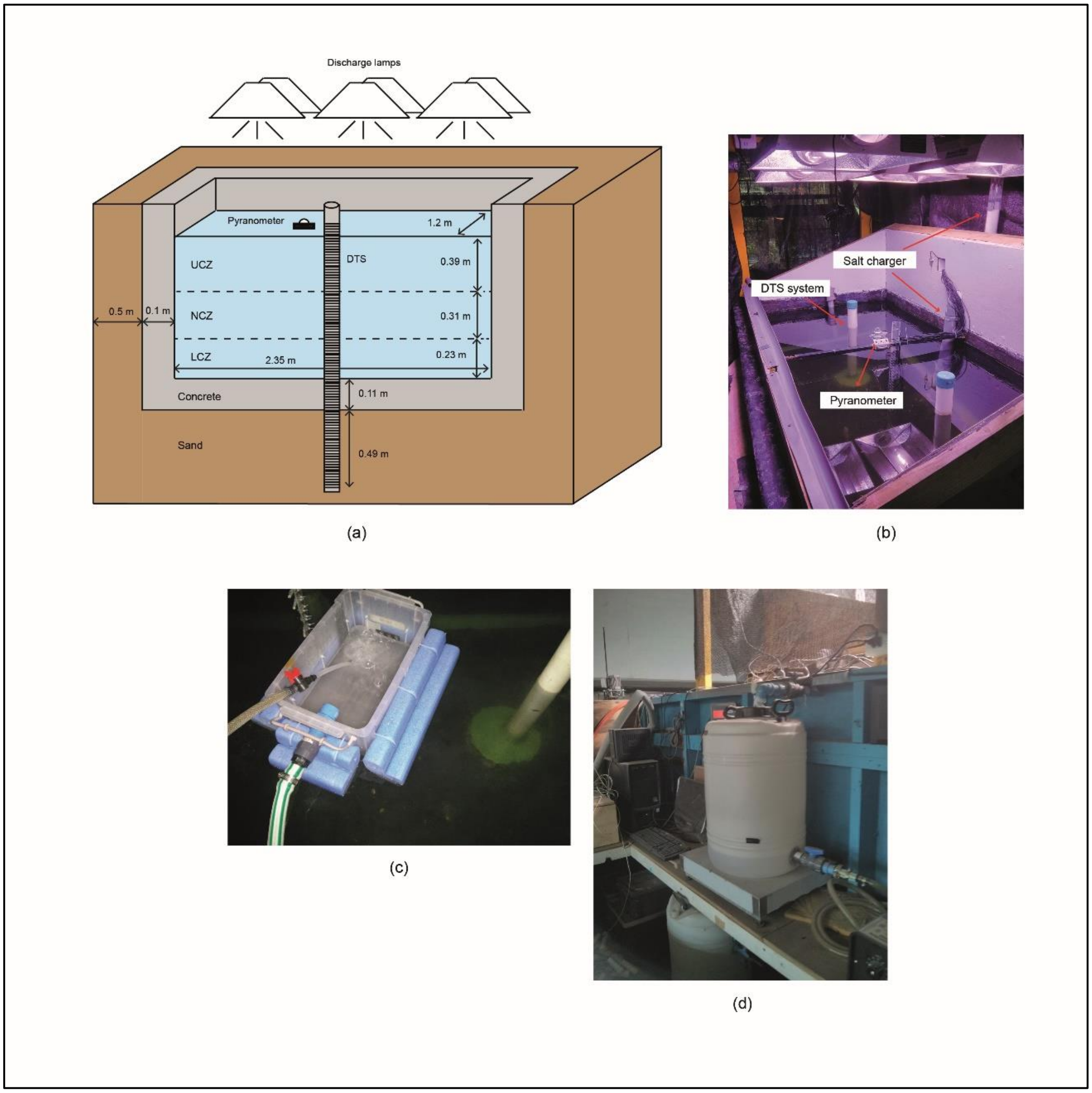

Figure 2-2:(a) Schematic view of the domain of the SGSP and the ground beneath. (b) Indoor experimental setup. (c) Floating diffuser used for pouring the salt solutions for creating the NCZ. (d) Water tank for monitoring evaporation losses.

2.4.4 Parameters calibration

Seven parameters of the model were calibrated as they were associated to specific conditions of the experimental SGSP, and performing a precise measurement of them was difficult. These parameters were the concrete, the moist sand and the dry sand's thermal conductivities (k_c, k_{ms}, k_{ds}), the convective heat coefficient for the SGSP and the ground perimeter ($U_{w,SGSP}$, $U_{w,g}$) and two parameters related with the radiation: the longwave absorption coefficient (β) and the extinction coefficient (η). These parameters were calibrated manually by minimizing the root mean square error (RMSE) between the observed and the simulated temperatures:

$$RMSE = \sqrt{\frac{1}{n}\sum_{i=1}^{n}\left(T_{obs,i} - T_{sim,i}\right)^2} \tag{1.15}$$

where $T_{obs,i}$ and $T_{sim.i}$ are the observed and the simulated temperature, respectively, at the i^{th} layer, and n represents the total amount of layers in the domain.

Three sets of experimental data were used for the calibration (Figure 1-3). The first set consisted in a period of 7.5 days in which the discharge lamps were powered off and the domain was restricted to the SGSP, i.e., the upper and lower boundaries were given by the SGSP's surface and bottom, respectively. The initial conditions for the water column's temperatures were obtained from the vertical high-resolution DTS measurements and corresponded to the end of a heating period, which implies that the temperatures in the SGSP were warmer than the ambient temperature. As the SGSP was inside a laboratory and surrounded with black curtains, incoming radiation from the sun was negligible in this period. In this way, parameters associated to the radiation did not have an impact in the model results and $U_{w,SGSP}$ was calibrated independently from the other parameters. During this cooling period, considering that no heat is gained from the ground to the SGSP and no radiative fluxes warm the deepest water layers, the LCZ is no longer a convective zone and therefore, it was treated as a purely conductive zone. To have a better representation of the conductive fluxes in the LCZ, this region was divided into multiple layers and it was treated as an extension of the NCZ, using equation (1.4).

The second and third datasets (Figure 1-3) were obtained from a 16-day time-period in which the discharge lamps were on continuously, with an average radiation of 309 W/m^2. In the second dataset, the domain was restricted to the ground beneath the SGSP, covering an 11-cm section of concrete and a 50-cm section of sand beneath it. Figure 1-4 shows the experimental temperature evolution in the ground beneath the SGSP during this time-period for different times. Two notorious slope changes can be identified in the temperature profiles. As the heat transport in the ground is governed by conduction, the multiple slopes are given by the different thermal conductivities of the materials. The first change in the slope of the temperature profile occurs 11 cm beneath the SGSP, and it is given by the concrete-sand interface. Nevertheless, a second slope change is observed, approximately 21 cm beneath the SGSP bottom. Considering that the domain beneath the concrete is only composed by sand, it was assumed that the different thermal conductivities between the first 10 cm of sand and the deeper sand layers are due to considerable changes in the soil water content. Thus, the sand region was divided into two sections: the first shallower section is called dry sand (*ds*) and the second deeper section, moist sand (*ms*). As the radiation parameters do not have an impact in the ground's temperature prediction, they were not required for this part of the calibration. In this way, four parameters were calibrated with the second dataset: the different thermal conductivities of the ground (k_c, k_{ds} and k_{ms}) and the ground's perimeter convective heat transfer coefficient ($U_{w,g}$).

In the third dataset, the domain was restricted to the SGSP. All the previously calibrated parameters were remained fix and the only parameters calibrated using this dataset were those associated to radiation absorption (η and β).

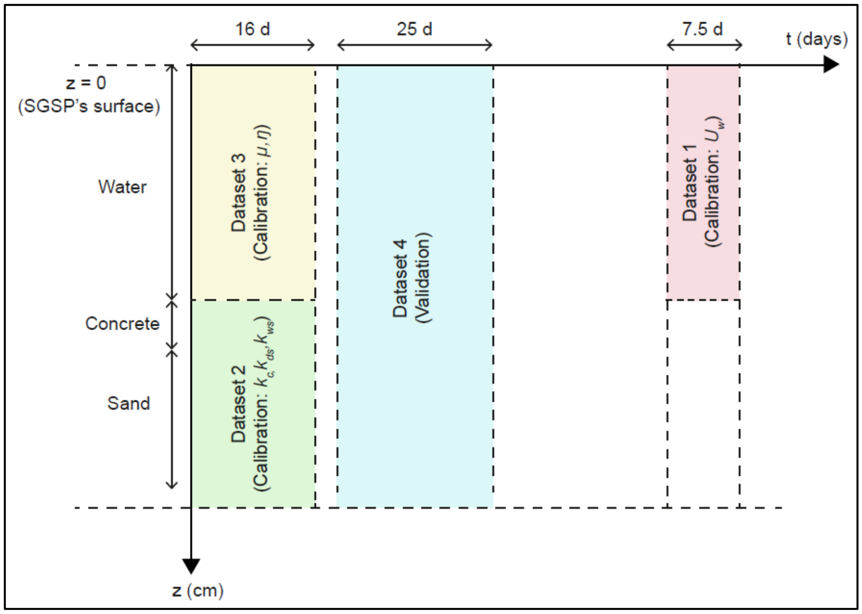

Figure 2-3: Experimental data measured from Santiago's SGSP used for the model calibration and validation.

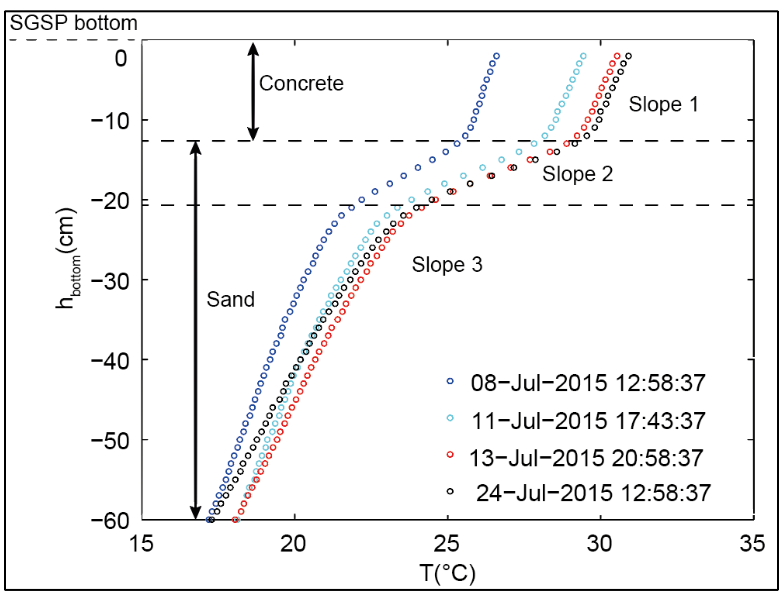

Figure 2-4: Temperature distribution in the ground beneath the SGSP in different times.

2.5 Results and discussion

2.5.1 Model calibration

The observed and predicted temperatures for the first, second and third datasets are shown in Figures 1-5(a), 1-5(b) and 1-5(c), respectively. To illustrate the thermal evolution, each figure shows three different days of operation. The modeled temperatures of the ground beneath the SGSP (Figure 1-5(b)) show the best agreement with the experimental temperatures, with an average RMSE of 0.2°C. Modeled temperatures for the SGSP instead (Figures 1-5(a) and 1-5(c)), have larger RMSE's. These large RMSE's can be explained because the heat transport representation in the SGSP is more complex than that in the ground because of two main reasons: (i) heat losses to the atmosphere are estimated using multiple parameters obtained from specific previous experiences, (ii) the uniform distribution of temperatures in the UCZ and the LCZ is based on the assumption that they are completely mixed convective zones and consequently, these temperatures have an additional uncertainty when these regions do not behave as uniform zones. Table 1-1 shows the different values for the calibrated parameters that minimized the different RMSE's. To verify the physical meaning of the calibrated parameters, these were compared with theoretical values or values reported in the literature. With the exception of $U_{w,g}$, all the parameters showed a good agreement.

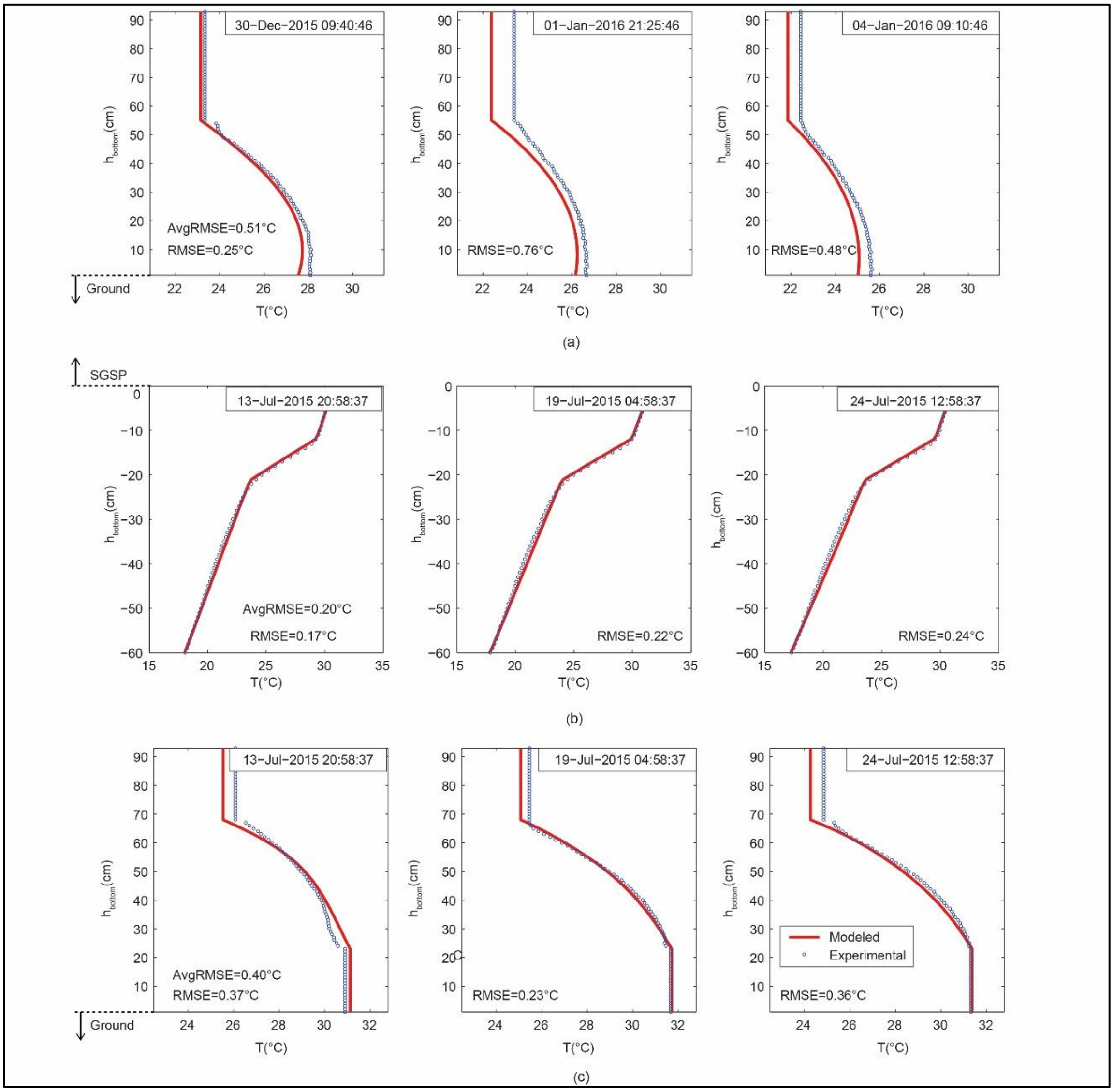

Figure 2-5: (a) Calibration of the wall's convective heat coefficient. (b) Calibration of the thermal conductivities in the ground beneath the pond and the ground's perimeter convective coefficient. (c) Calibration of the radiation's parameters.

Based on the calibration results, the best fit is obtained when the ground perimeter heat fluxes are considered null, i.e., $U_{w,g} = 0$. This null heat flux can be explained because the DTS system used for measuring the ground's temperatures was positioned in the middle part of the domain (Figure 1-2(b)), resulting in an overestimation of the average ground's temperatures, as the perimeter heat losses are less perceived. Analogously, temperatures measured in the SGSP are also an overestimation, but in a lesser extent than the ground, as the heat transport in the UCZ and the LCZ occurred by convection, which contributed to a larger heat transport inside those zones.

Table 2-1: Calibrated parameters compare to literature and theoretical values

Parameter (units)	**Symbol**	**Calibrated value**	**Literature or theoretical value**
Wall's convective heat coefficient (W m^{-2} K^{-1})	$U_{w,SGSP}$	0.8	0.6 (equation (1.14))
Ground's perimeter convective heat transfer coefficient (W m^{-2} K^{-1})	$U_{w,g}$	0	0.4 (equation (1.14))
Concrete's thermal conductivity (W m^{-1} K^{-1})	k_c	1.4	1.15-1.65 (Chen, 2008)
Moist sand's thermal conductivity (W m^{-1} K^{-1})	k_{ms}	1.2	0.3-2 (ISO, 2007)
Dry sand's thermal conductivity (W m^{-1} K^{-1})	k_{ds}	0.3	0.15-0.3 (ISO, 2007)
Absorption coefficient (-)	μ	0.68	0.5 (Kurt et al., 2006)
Extinction coefficient (m^{-1})	η	1.3	1.04 (Ruskowitz et al., 2014)

2.5.2 Model validation with experimental SGSP

The same experimental SGSP used to calibrate the model was used to validate it with a fourth dataset (Figure 1-3). For a period of 28 days, the discharge lamps were programmed in a 12-12 configuration, i.e., they were powered on for 12 hours and powered off for the rest 12 of the day to mimic a daily cycle. Figure 1-6(a) shows the radiative fluxes measured by the pyranometer during a period of 44 days. The first 16 days correspond to the calibration period and the remaining 28 days to the validation period. The average radiation during the validation period was 251 W m^{-2}, with fluxes ranging between 0 and 459 W m^{-2}. The spatial domain considered in the fourth dataset was given by the SGSP, the concrete and the sand beneath it. As the experimental temperatures in the convective zones were not completely uniform, the average experimental temperature was calculated for the UCZ and the LCZ to compare them to the modeled temperatures. Figure 1-6(b) illustrates the modeled and observed temperature evolution in both regions. It is observed that the RMSE for the validation period for both UCZ and LCZ increases in comparison to the calibration period. In the UCZ, the RMSE is equal to 1.35°C. In this zone, both experimental and modeled temperatures have a similar trend. Nevertheless, experimental temperatures show a larger variability during the daily cycle, reaching higher temperatures during the day and lower temperatures during the night. The different amplitude in the oscillations of the modeled and experimental UCZ temperatures can be explained because the air temperature used for the model's upper boundary condition could have been affected by the heat fluxes coming from the SGSP's surface and the higher amount of water vapor retained in the air. Therefore, as the specific humidity in the air near the pond is expected to be higher, so is the specific heat and more energy is necessary to vary the temperature of a certain mass of air. Because of this, the modeled temperature oscillations of the air near the surface of the SGSP are expected to be smaller than the real ambient temperature oscillations. Temperatures in the LCZ instead, maintain a lower RMSE of 1.13°C, which is considered good.

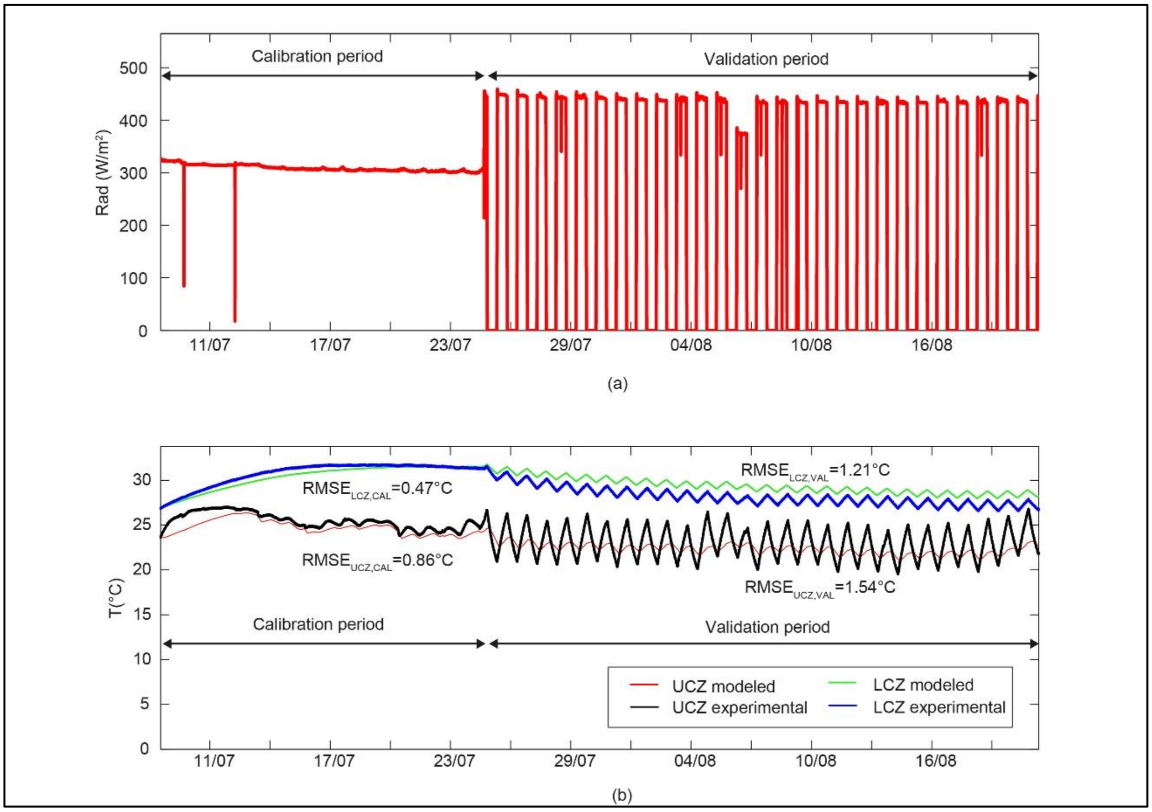

Figure 2-6: (a) Radiative fluxes during the calibration and validation periods. (b) Temperature evolution in the UCZ and the LCZ, in Santiago's experimental SGSP.

Figures 1-7(a) and 1-7(b) show the modeled and experimental thermal evolution of the whole domain during the 44 days of simulation. A similar trend is observed between modeled and observed temperatures. The experimental data prove that the UCZ and LCZ act as convective zones as the temperatures tend to be uniform inside those regions. Nevertheless, during the validation period, the UCZ's temperatures were less uniform, as the first centimeters of the UCZ were more sensible to atmospheric changes. This sensitivity occurred due to the operating conditions of the validation period, in which events with smaller time scales than the model time steps occurred. For instance, when the lamps were turned on, the top of the UCZ received abruptly the incoming radiation as the flux changed from 0 W/m^2 to over 300 W/m^2 in a time interval shorter than 1 min. A similar situation happened when the lamps were turned off, as the radiation decreased abruptly to zero. The LCZ instead, is less affected by the abrupt change in the incident radiation, as the NCZ and the UCZ attenuate the radiative fluxes. Based on equation (1.5) and the calibrated parameters (η and μ), only 40.5% of the radiation that penetrates the SGSP's surface, is received by the LCZ.

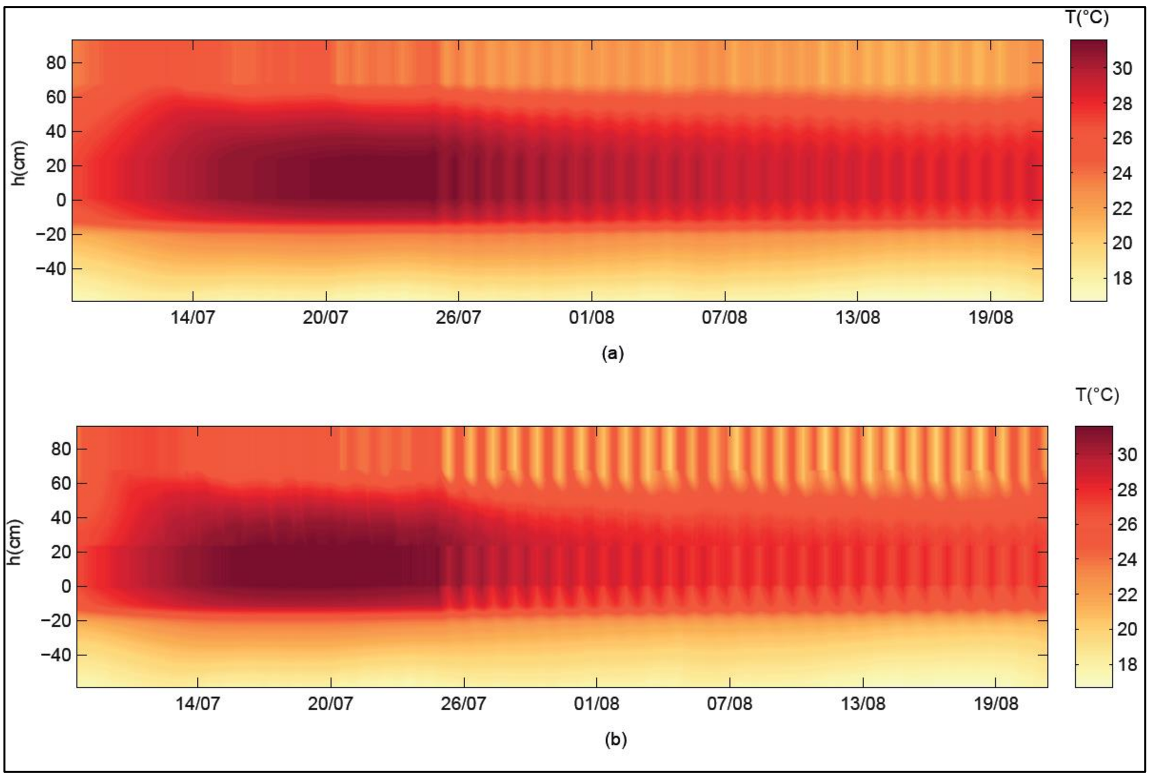

Figure 2-7: Modeled (a) and experimental (b) evolution of temperatures in the water and the ground beneath, in Santiago's experimental SGSP.

2.5.3 Model validation with data from the SGSP literature

The model was validated with experimental data from three SGSPs. These ponds are located in El-Paso, USA (Lu et al., 2001), Kuwait City, Kuwait (Ali, 1986) and Barcelona, Spain (Valderrama et al., 2011). Contrary to our laboratory conditions, these three SGSPs were exposed to atmospheric conditions, i.e., they were heated with natural solar radiation. The validation period for each solar pond used 1-year datasets and, where no heat was extracted from the SGSPs. The dimensions of the different SGSPs are presented in Table 1-2. Further, monthly average meteorological data used for the upper boundary condition in the three SGSPs is summarized in Table 1-3.

Table 2-2: Dimensions of the different SGSPs.

SGSP	El Paso	Kuwait City	Barcelona
Area (m^2)	3,000	8	50
Perimeter (m)	260	12	25.1
UCZ thickness (m)	0.7	0.2	0.3
NCZ thickness (m)	1.2	0.4	1.7
LCZ thickness (m)	1.35	0.3	0.8
Buried	Yes	Yes	No

Table 2-3: Summary of the meteorological conditions of the different SGSPs.

SGSP	Month	Radiation (W/m^2)	Relative humidity (%)	Wind speed (m/s)	Air temperature (°C)
El Paso, USA (1999)	Jan	145.8	51	3.2	6
	Feb	187.5	42	3.5	8.9
	Mar	245.8	32	4.4	12.8
	Apr	295.5	27	4.4	17.4
	May	325.0	27	4.1	22.1
	Jun	333.3	30	3.5	26.9

	Jul	308.3	44	3.2	27.9
	Aug	283.2	48	3	26.7
	Sep	245.8	51	2.9	23.6
	Oct	204.1	47	2.8	17.8
	Nov	158.2	47	3.1	11.3
	Dec	133.1	52	3	6.7
Kuwait City, Kuwait (2000)	Jan	133.3	53.6	3.3	12.6
	Feb	176.3	43.7	3.5	14.6
	Mar	210.4	37.9	3.7	19.1
	Apr	243.3	29	3.4	25.9
	May	292.1	20.4	4.1	32
	Jun	328.8	15.3	4.5	35.7
	Jul	318.3	15.2	4.2	37.6
	Aug	297.1	17.4	4.1	37.2
	Sep	256.7	20.6	3.7	33.6
	Oct	196.7	30.1	3.3	28.1
	Nov	135.0	43.2	3.4	20.5
	Dec	110.4	51.5	3.4	14.7
Barcelona, Spain (2009-2010)	Nov	80.4	75	3.7	12.0
	Dec	63.1	73	4.3	7.9
	Jan	71.4	73	4.1	7.1
	Feb	95.0	74	5.1	7.4
	Mar	168.3	69	5.1	9.9
	Apr	204.3	63	5.1	14.3
	May	213.0	53	5.1	16.7
	Jun	212.1	48	5.3	21.5
	Jul	235.6	43	6.1	26.8
	Aug	206.5	45	5.3	25.3
	Sep	153.1	53	4.7	21.4
	Oct	116.8	65	4.7	15.9

Figures 1-8(a), 1-8(b) and 1-8(c) show the experimental and modeled temperatures for the UCZ and the LCZ for SGSPs at El Paso, Kuwait City and Barcelona, respectively. In comparison to the experimental SGSP built for this study, the model’s RMSE with the literature SGSPs is bigger, going from 2.5°C (UCZ of Barcelona's SGSP) to 7.6°C (LCZ of Kuwait City's SGSP). The error for the three cases is bigger in the LCZ, which is given in part due to the lack of information of the ground thermal properties. As the heat losses to ground have a big impact in the LCZ's temperature, not having a good representation of the ground results in a worse prediction of temperatures in the LCZ. Nevertheless, the modeled temperatures can be a good first approximation, considering that only monthly average values were used for the model's input and results can be improved with more detailed information.

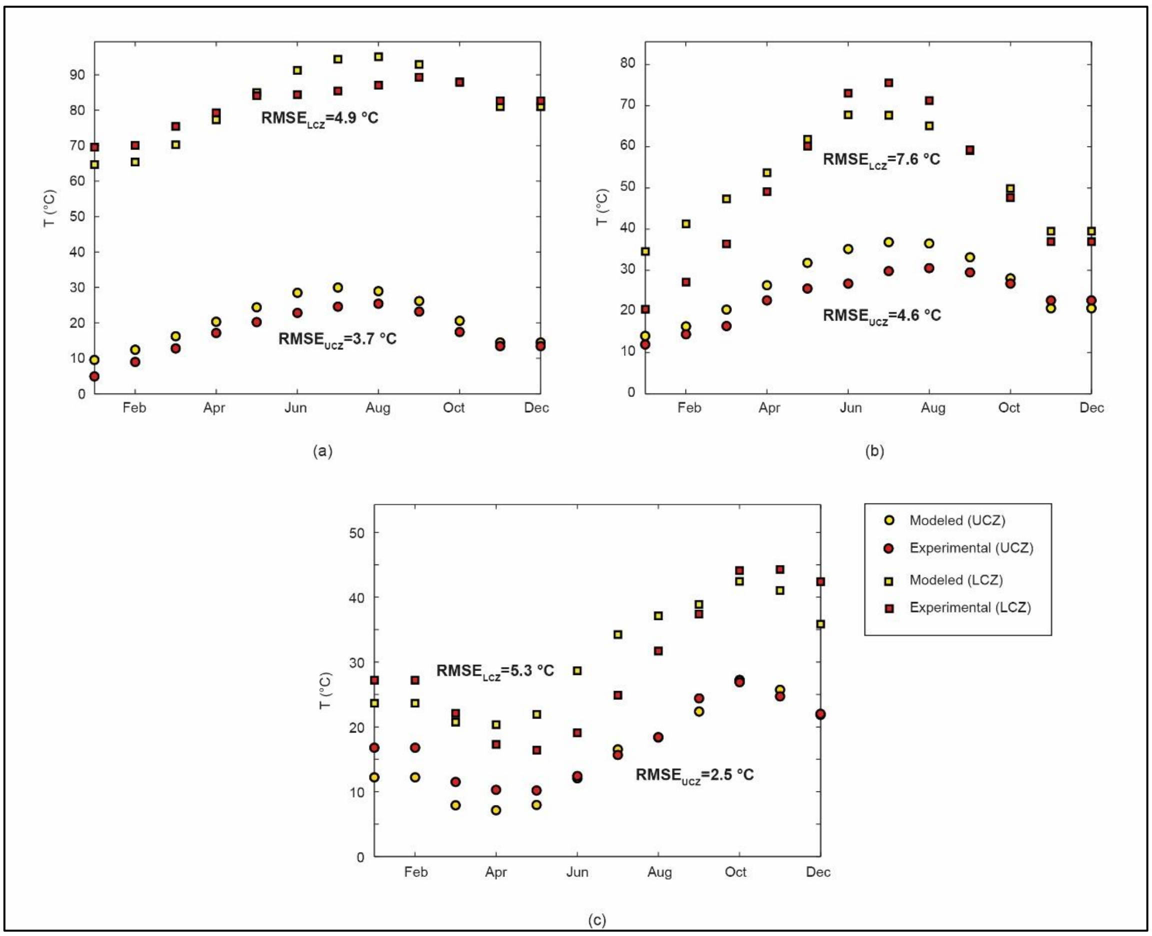

Figure 2-8: Model validation: (a) El Paso; (b) Kuwait City; (c) Barcelona.

2.5.4 Ground heat fluxes

To demonstrate the relevance of dividing the ground beneath an SGSP into multiple layers, a hypothetical scenario with heat extraction from the LCZ was simulated. For that purpose, the El Paso's SGSP was modeled and a constant heat flux of 40 W/m^2 was continuously removed from the LCZ during a period of three years. To simplify the study, details of the method used for heat removal were not included as they are not relevant in the thermal analysis. Further, it was assumed that the groundwater table was 20 m deep and had a constant temperature of 17 °C.

Figure 1-9 shows the heat fluxes in the boundary between the SGSP's bottom and the ground beneath it. The blue line represent the results obtained with the present model (equation (1.10)), where the ground was divided into multiple layers. During the winter period, the heat flux comes from the ground to the LCZ because the ground stores heat from the warmer previous months, and then releases this heat when the LCZ has lower temperatures. According to Sezai and Tasmdemiroglu (1995), ground storage is more efficient when heat is removed from the SGSP. The red line instead, represents the ground heat fluxes when ground is treated as a single layer as assumed in (Sayer et al., 2016), calculated with the following equation:

$$Q_g = U_g\left(T_L^{n+1} - T_{gw}\right) \qquad (1.16)$$

where U_g is the overall heat transfer coefficient for the ground between the SGSP and the groundwater table, calculated with equation (1.14). Given that the groundwater temperature was always smaller than the LCZ's temperature, heat fluxes were constantly negative, i.e., they were lost from the LCZ to the ground. Because of this, ground heat storage cannot be represented when this approach is used. This can have a negative effect in the LCZ temperature prediction, because heat recovery from the ground during the winter periods stabilizes the temperatures in the SGSP through the year (Zhang and Wang, 1990).

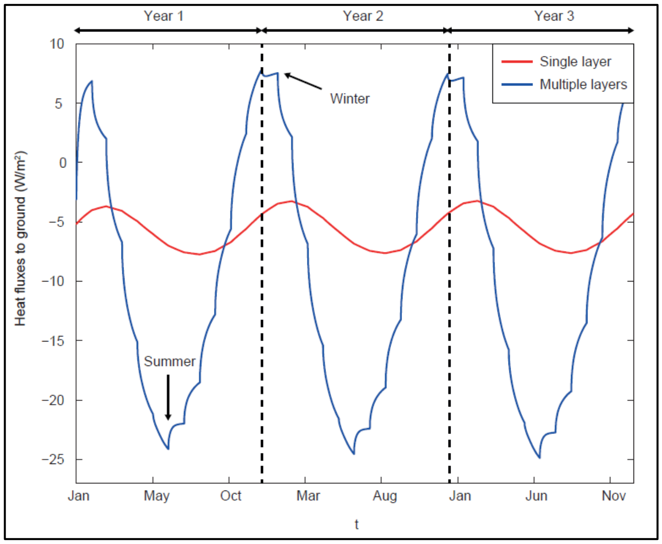

Figure 2-9: Comparison of the heat fluxes in the boundary between El Paso's SGSP and the ground beneath, when the ground is divided into multiple layers (present work) and when the ground is treated as a single layer.

2.6 Conclusions

In this study a simplified one-dimensional transient model to predict the temperatures distribution in a SGSP and the ground beneath it was developed. The model was calibrated and validated with an experimental SGSP heated with high-intensity discharge lamps. The agreement between experimental and modeled temperatures was very good, with a RMSE's of 1.35 and 1.13 °C in the UCZ and LCZ, respectively. Further, it was demonstrated that the model also correctly predicted the temperature evolution of three different SGSP exposed to natural solar radiation.

Even though small heat fluxes through the ground's perimeter of the experimental SGSP were expected, they could not be perceived, because the DTS system was positioned in the center of the SGSP. Nevertheless, considering the small dimensions of the experimental SGSP used in this investigation (~2.82 m^2) compared to a large-scale SGSP (~1,000-100,000 m^2), neglecting the ground's perimeter heat losses in the practice can be a good approximation.

The use of multiple layers to represent the ground beneath a SGSP showed to be a good feature to incorporate in unsteady SGSP's models, as they allow the simulation of the ground heat storage, which is important to consider as it contributes to more stable temperatures in the SGSP and enhances the operation

2.7 Appendix A. Heat loss to atmosphere

A.1 Evaporation heat flux (Q_e)

Heat loss by evaporation is given by the following expression (Adams et al., 1990):

$$Q_e = (Q_{free}^2 + Q_{forced}^2)^{\frac{1}{2}} \tag{1.17}$$

where Q_{free} and Q_{forced} are free and forced convection, respectively, and are calculated using equations (1.18)-(1.25):

$$Q_{free} = \begin{cases} 2.7 * 10^{-2}(T_{wv} - T_{av})^{\frac{1}{3}} * (e_{sw} - e_a) & ,if \;\; T_{wv} > T_{av} \\ 0 & ,if \;\; T_{wv} \leq T_{av} \end{cases} \tag{1.18}$$

$$Q_{forced} = 3.1 * 10^{-2} U_2 (e_{sw} - e_a) \tag{1.19}$$

$$T_{wv} = \frac{T_w}{1 - \frac{0.378}{P_{atm}} e_{sw}} \tag{1.20}$$

$$T_{av} = \frac{T_a}{1 - \frac{0.378}{P_{atm}} e_a} \tag{1.21}$$

$$e_{sw} = 2.718 * 10^{10} \exp\left(\frac{-4,157}{T_w + 239.24}\right) \quad (1.22)$$

$$e_a = hr * e_{sat} \quad (1.23)$$

$$e_{sat} = 2.718 * 10^{10} * \exp\left(\frac{-4,157}{T_a + 239.24}\right) \quad (1.24)$$

$$P_{atm} = 101,300 * \exp\left(\frac{-h}{8.200}\right) \quad (1.25)$$

A.2 Long-wave radiation flux (Q_l)

Long-wave radiation fluxes in the boundary between the SGSP's surface and the ambient is given by the difference between the long-wave radiation from water to the atmosphere (Q_{lw}) and the long-wave radiation from the atmosphere to the water (Q_{la}):

$$Q_l = Q_{lw} - Q_{la} \quad (1.26)$$

$$Q_{lw} = \epsilon_w \sigma (T_u + 273,15)^4 \quad (1.27)$$

$$Q_{la} = \epsilon_a \sigma (T_a + 273,15)^4 \quad (1.28)$$

The air's emissivity is calculated according to Raphael's expression (Henderson-Sellers, 1986):

$$\epsilon_a = 1 - 0,26 * \exp(-7,77 * 10^{-5} e_a^2) \quad (1.29)$$

A.3 Sensible heat flux (Q_s)

The sensible heat flux is calculated with the following equation (Losordo and Piedrahita, 1991):

$$Q_s = 1.5701 * U_2 (T_w - T_a) \quad (1.30)$$

3 THE ROLE OF THE GROUND HEAT STORAGE CAPACITY ON THE OPERATION OF A SOLAR POND

3.1 Abstract

Salt-gradient solar ponds are large-scale low-cost solar collectors and storage systems that provide a continuous heat supply for low-temperature thermal applications. Although many studies have investigated the thermal behaviour of solar ponds, few researches have investigated how the heat collected in the ground beneath a pond can be recovered during heat extraction. In this work, a one-dimensional transient model is used to study the thermal interaction between a solar pond and the ground beneath it, and an algorithm was developed for operating the pond with constant heat extraction from its bottom layer. Simulation results demonstrate that adding an insulation layer is not economically convenient under these operation conditions. Further, it is observed that when no insulation is used, the ground below the pond acts as an additional heat storage volume, permitting more stable temperatures through the year and recovering 25.5% of the heat that was stored in the ground during the winter period. A sensitivity analysis showed that the pond's temperature has a linear relation with the ground's thermal conductivity and a logarithmic relation with the water table depth.

Keywords: Solar pond, heat extraction, solar energy, ground storage.

3.2 Introduction

Salt-gradient solar ponds (SGSPs) are low-cost solar collectors, with long-term heat storage capacity that can deliver heat during the day and the night (Prasad and Rao, 1993). SGSPs have become an attractive technology in locations that have high solar irradiance, excess water and excess salts. A SGSP generally has three characteristic zones (Figure 2-1). The upper convective zone (UCZ), located at the top of the pond, is a thin and uniform layer of fresh water or low salt concentration (0–4 %w) with a typical thickness ranging between 0.1 and 0.4 m. The intermediate zone, called non convective zone (NCZ), is formed by a constant salinity that increases the salt concentration within the pond as the depth increases. Its thickness varies depending on the desired temperature and heat extraction rate (Hull et al., 1989). The bottom part, called storage zone or lower convective zone (LCZ), is formed by a high salinity solution (21–26 %w) and its thickness typically varies between 0.8 and 1.2 m. As the salts in the solar pond are completely dissolved, the water is transparent and allows radiation to penetrate into the deepest layer of the pond. The salinity gradient acts as a transparent insulator for the LCZ. It permits the sunlight to travel until the pond’s bottom, but it suppresses the global circulation within the pond because the salt gradient counteracts the buoyancy effect of the warmer water below (Saleh et al., 2011). Thus, the only heat losses from the LCZ to the atmosphere occur by conduction, but the relatively low thermal conductivity and high heat capacity of the brine allows collecting heat at the bottom of the pond, which makes the SGSP a long-term heat storage device (Lu et al., 2001).

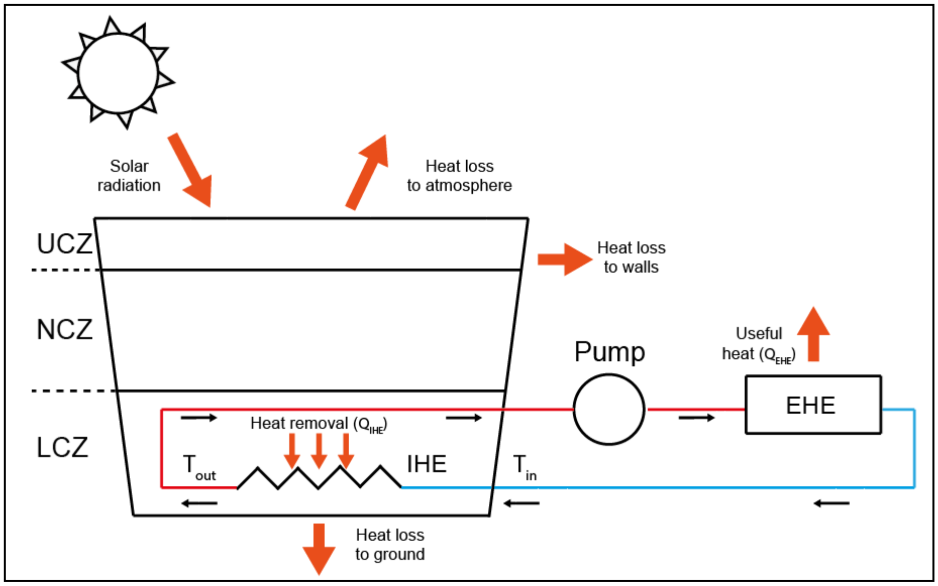

Figure 3-1: Characteristic zones in an SGSP and heat removal from the LCZ.

The highest temperatures inside the SGSP are achieved in the LCZ, with typical temperatures ranging between 70 and 90 °C (Abdullah et al., 2016), which imply that an important part of the stored heat may be lost to the ground. The addition of an insulation layer at the bottom of the pond is a common practice to reduce ground heat losses, but there are no studies that have analyzed its effect on pond performance when heat is extracted at a constant rate from the bottom of the pond. The objectives of this work are to study the heat storage capacity of the ground beneath a SGSP and to understand the impact of an insulation layer on the pond's performance. To achieve these objectives, a one-dimensional transient model was used to describe the thermal behaviour of an SGPS and the ground beneath it. Using this model, the thermal evolution of a solar pond located in Copiapó, Chile was simulated, and an algorithm was proposed to have a constant heat extraction from the LCZ. Finally, an economic analysis was made to determine the convenience in the use of an insulation layer.

3.3 Materials and methods

3.3.1 Thermal model

The temperature evolution in a SGSP and the ground beneath it can be represented by a one-dimensional transient model using the finite difference method (Date et al., 2013; Sayer et al., 2016; Wang and Akbarzadeh, 1982). The model developed for this investigation uses an energy balance in each node within the domain to describe the thermal dynamics (Date et al., 2013):

$$\Delta E_n^{t+\Delta T} = \rho_n c_{P,n} \Delta z_n A_{sp} = \sum Q_{in,n} - \sum Q_{out,n} \tag{2.1}$$

where $\Delta E_n^{t+\Delta T}$ is the change in the energy content in the nth layer after an interval of ΔT time; t is time; Δz is the layer's thickness; ρ_n and $c_{P,n}$ are the layer's density and specific heat, respectively, A_{sp} is the SGSP's area and $Q_{in,n}$ and $Q_{out,n}$, are the incoming and outgoing energy fluxes from the nth layer, respectively.

The model assumes that both the UCZ and LCZ are completely mixed, i.e., their temperatures are uniform. The top boundary conditions include heat losses by convection, sensible heat and longwave radiation to the atmosphere. These heat fluxes are modelled with the expressions proposed by (Adams et al., 1990; Henderson-Sellers, 1986). The shortwave radiation attenuation through the water column is represented by Beer's law (Kurt et al., 2006). Heat loss from the SGSP to the ground, $Q_{LCZ/g}$, is treated as a convective loss according to:

$$Q_{LCZ/g} = h_1 \left(T_{g,1} - T_{LCZ} \right) \tag{2.2}$$

where $T_{g,1}$ is the temperature of the shallowest ground layer beneath the SGSP, T_{LCZ} is the temperature of the LCZ and h_1 is the convective heat coefficient between the LCZ and the bottom of the SGSP, assumed to be equal to 78.12 W/m^2 K (Sodha et al., 1980).

Furthermore, heat transport to deeper ground layers occur only by conduction and is represented using Fourier's Law:

$$Q_{g,i} = k_g \left(\frac{T_{g,i-1} - T_{g,i}}{\Delta z_i} \right) \tag{2.3}$$

where $Q_{g,i}$ is the heat flux through the ground, from the ith layer to the layer beneath it and k_g is the ground's thermal conductivity. At a certain lateral distance x_g (Figure 2-2), heat fluxes coming from the pond are negligible and the temperature in the ground can be considered constant and equal to the yearly average of the ambient (T_{avg}) (Date et al., 2013). Lateral heat conduction fluxes from the ground layers are treated as convective fluxes:

$$Q_w(z,t) = U_w \left(T_{avg} - T(z,t) \right) = \frac{x_g}{k_g} \left(T_{avg} - T(z,t) \right) \tag{2.4}$$

where U_w is the overall heat transfer coefficient between the pond's wall and the boundary of the SGSP's heat field. The deepest ground layer in the model limits with the water table at its bottom. Heat losses from the ground to the water table, $Q_{g/WT}$, are treated as convective fluxes according to:

$$Q_{g/WT} = h_2 \left(T_{gw} - T_{g,N} \right) \tag{2.5}$$

where T_{gw} is the groundwater temperature, T_N is the temperature of the deepest ground layer and h_2 is the convective heat coefficient at the phreatic surface, assumed to be equal to 185.8 W/m^2 K (Sodha et al., 1980). The development of the model, its calibration and validation were performed using an experimental SGSP that was built on Santiago and are presented elsewhere (Chapter 1).

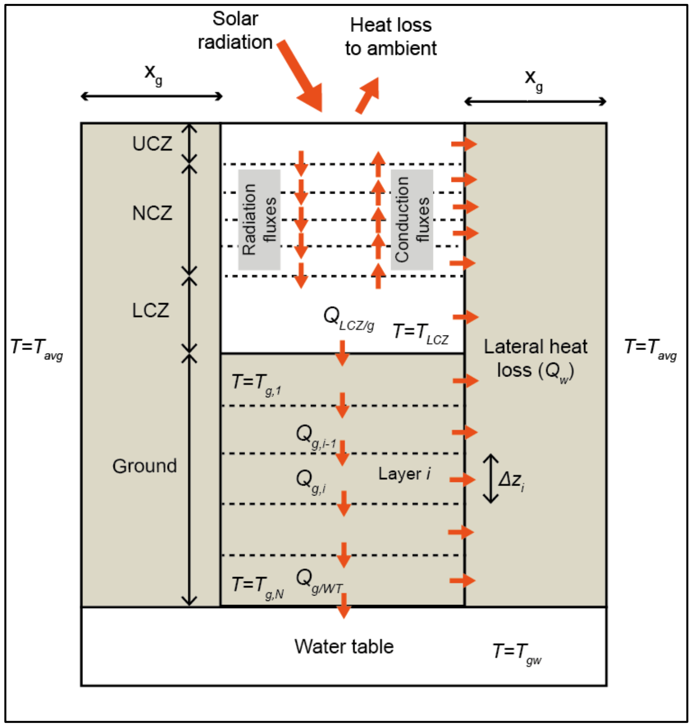

Figure 3-2: Heat fluxes representation in the developed model.

3.3.2 Simulation conditions

To understand the role of ground heat storage on the operation of a solar pond, the thermal evolution of a 20.000-m^2 solar pond located in Copiapó, Chile (27°57’32”S, 70°0’36”W) was simulated for a period of 5 years. After the maturation period (six months), heat was removed from the LCZ at a constant rate.

The hourly meteorological conditions of Copiapó were used to estimate the boundary conditions at the top of the pond. As a reference, the monthly average climate conditions for a representative year in Copiapó are shown in Table 2-1. The SGSP was assumed to have 0.10-m concrete walls (k_c=1 W/m°C, ρ_c=880 kg/m^3, C_{Pc}=2,230 J/kg°C). The ground in which the pond is buried is clay (k_g=1 W/m°C, ρ_g=880 kg/m^3, C_{Pg}=2,230 J/kg°C

(Zhang and Wang, 1990)) and the water table is 35 m below the bottom of the pond (DGA, 2004). The temperature of the groundwater table is used as lower boundary condition, which is assumed to be constant and equal to 24.3 °C (Soto, 2010). The UCZ thickness was set at 0.3 m and the LCZ at 1.0 m (Garrido and Vergara, 2013). The NCZ thickness was 1.2 m, and was defined to maximize the LCZ temperatures.

Table 3-1: Climate conditions of Copiapó, Chile.

Month	Solar radiation (W/m^2)	Air temperature (°C)	Wind speed (m/s)	Relative humidity (%)
January	329.3	22.0	2.2	39.4
February	298.6	21.0	2.2	40.6
March	249.5	19.3	1.8	47.5
April	226.0	16.9	1.4	49.0
May	168.0	14.5	1.3	40.8
June	154.6	14.2	1.5	23.1
July	159.4	14.4	1.5	22.6
August	195.3	16.1	1.5	28.1
September	245.5	16.4	1.6	30.4
October	291.8	18.0	1.7	33.3
November	337.3	18.8	1.9	34.2
December	347.8	20.9	2.1	36.0

3.3.3 Heat extraction

A conventional method for heat extraction was used (Leblanc et al., 2011). Heat was withdrawn from the LCZ using an internal heat exchanger (IHE). A heat transfer fluid is circulated in a closed cycle through the IHE and the transferred thermal energy is then extracted using an external heat exchanger (EHE) (Leblanc et al., 2011), as shown in Figure 2-1. For the present study, seawater is used as the transfer fluid. The thermal energy extracted from the IHE and the EHE, can be calculated with the following equations (Jaefarzadeh, 2006):

$$Q_{EHE} = \frac{\dot{m}C_P(T_{out} - T_{in})}{A} \tag{2.6}$$

$$T_{out} = T_{LCZ} - \frac{T_{LCZ} - T_{in}}{\exp\left(\frac{U_{IHE}A_{IHE}}{\dot{m}C_P}\right)} \tag{2.7}$$

$$U_{IHE} = \frac{1}{\frac{d_e}{d_i}\frac{1}{h_i} + \frac{d_e}{2k_p}\ln\left(\frac{d_e}{d_i}\right) + \frac{1}{h_e}} \tag{2.8}$$

where $\dot{m}$ is the mass flow rate; C_P the specific heat of the circulating water and T_{in} and T_{out} are the temperatures of the water before and after being pumped through the IHE; T_{LCZ} is the LCZ's temperature; A_{IHE} the resulting area of the IHE and U_{IHE} the overall coefficient of heat transfer of the IHE, which is calculated with equation (2.9); d_i and d_e are the internal and external diameters of the IHE pipes. The IHE design is similar to the one used at the Pyramid Hill's solar pond (Leblanc et al., 2011), with 40 200-m long heat extraction polyethylene tubes (k_p=0.37 W/m°C), all connected to two manifold pipes. The convective coefficients of the heat transfer fluid inside (h_i) and outside the IHE (h_e) are 5,000 and 1,500 W/m^2°C, respectively.

Due to the intermittent nature of the solar radiation, one of the biggest challenges of solar technologies is to continuously supply energy for long time periods, which implies that heat must be extracted during the night. Because of this issue, as an operation restriction, the heat removal from the LCZ is performed at a constant rate of 35 W/m^2. To achieve this constant heat rate extraction, the mass flow rate through the heat exchangers has to vary in time according to the LCZ temperature. A four-step iteration method is used to determine the mass flow rate for each time step. This method is illustrated in Figure 2-3. For a given time and desired heat extraction rate (Q_{OP}), the model settles an arbitrary value for the mass flow rate in order to initialize the iteration (Step 1). Using equation (2.7), the fluid's temperature at the outlet of the IHE is calculated (Step 2). Then, with equation (2.8), the model calculated the extracted heat rate with the EHE (Q_{EHE}) (Step 3). If the differences between Q_{EHE} and Q_{OP} is larger than 0.01 W/m^2, the model recalculates the mass flow rate as a function of Q_{OP} and T_{out}, by reassembling equation (2.8) (Step 4), and goes back to Step 2. This loop is maintained until Q_{EHE} converges to Q_{OP} and the mass flow rate for a certain time step will be the value that meets the convergence criteria.

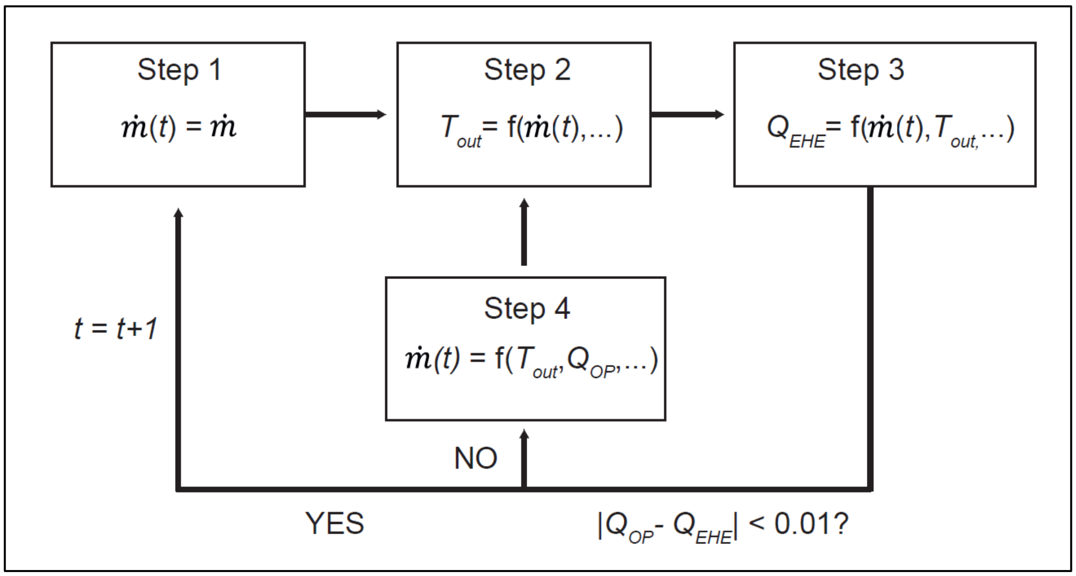

Figure 3-3: Four-step algorithm to determine the mass flow rate that results in a constant heat extraction.

3.3.4 Insulation layer

An economic evaluation of a polystyrene insulation layer (k_i=0.03 W/m°C, ρ_i=35 kg/m^3, C_{Pi}=1,400 J/kg°C) was made. As the polystyrene density is lower than the brine's density, the insulation layer was located under the concrete layer in order to counteract the buoyancy force. The economic analysis considered a 20 years horizon, with a discount rate of 10%. The two main cash fluxes are given by the investment cost, which takes place only during the first year and the benefit of reducing the pumping cost, which is associated to the operation of the pond and therefore is considered for every year. Recall that it is considered that the heat extraction rate is constant. Therefore, for any configuration of the insulation layer the benefits associated with the extracted heat will be equal.

Investment cost: for the present study it is assumed that for each cubic meter of insulation layer, the total cost of the polystyrene and the excavation is 6 US$ (Garrido and Vergara, 2013).

Operation cost: when an insulation layer is added, the thermal evolution of the SGSP through time is different and so is the pumping cost to extract the same amount of energy (Q_{op}). The pressure loss through the IHE pipes, neglecting the minor losses, can be approximated with the following equation (Yunus and Cimbala, 2010):

$$\Delta P = \frac{8fL\left(\frac{\dot{m}}{N}\right)^2}{g\pi^2 {d_i}^5} \tag{2.9}$$

where *f* is the friction factor, which is calculated using the Swamee-Jain equation (Yunus and Cimbala, 2010); *L* is the total length of the pipe network; *N* is the total number of heat extraction pipes, g is the acceleration of gravity; and d_i is the internal diameter of the pipes. Finally, the electric power demand (W) for pumping a certain mass flow rate and its cost (US$) are given by equations (2.10) and (2.11), respectively:

$$P_{elec} = \frac{\dot{m}\Delta P}{\rho n_p n_t n_m} \tag{2.10}$$

$$C_{pump} = \frac{C_{kWh.} P_{elec} h}{1{,}000} \tag{2.11}$$

where n_p, n_t and n_m are the efficiency of the pump, the transmission and the electric motor, and are assumed to be 75, 90 and 90%, respectively (Vogelesang, 2008). The cost of producing 1 kWh (C_{kWh}) is assumed to be 0.166 US$/kWh, according to the marginal production cost of the power production plant nearest to Copiapó (Suárez et al., 2014b). As the internal diameter of the pipes is related with the frictional losses and eventually with the pumping cost, this dimension is defined to minimize the overall cost of investment and pumping. Based on the available diameters in the market, the optimum external diameter of the pipes is 63 mm, with a wall thickness of 3.8 mm.

3.4 Results and discussion

3.4.1 Base scenario: SGSP with no insulation

The thermal evolution of the LCZ and the heat fluxes from the pond to the ground, when no insulation layer is used, are illustrated in Figure 2-4(a). When quasi-steady state is reached, the annual average temperature of the LCZ is 65.3 °C, with a maximum of 76.5 °C and minimum of 53.3°C. As the heat removal rate is constant in time, the mass flow rate increases during the winter months, and decreases during the summer months (Figure 2-4(b)). This behavior occurs because in winter the pond has lower temperatures and in summer the pond has higher temperatures. Furthermore, when no insulation is used, the ground beneath the SGSP acts as an additional heat storage volume, permitting more stable temperatures in the LCZ throughout the year. During the winter period, when the pond has the lowest temperatures, the heat stored in the ground flows from the ground to the LCZ. In quasi-steady regime, 25.5% of the heat lost to the ground is recovered back to the pond in the winter period, with fluxes of up to 3.9 W/m^2.

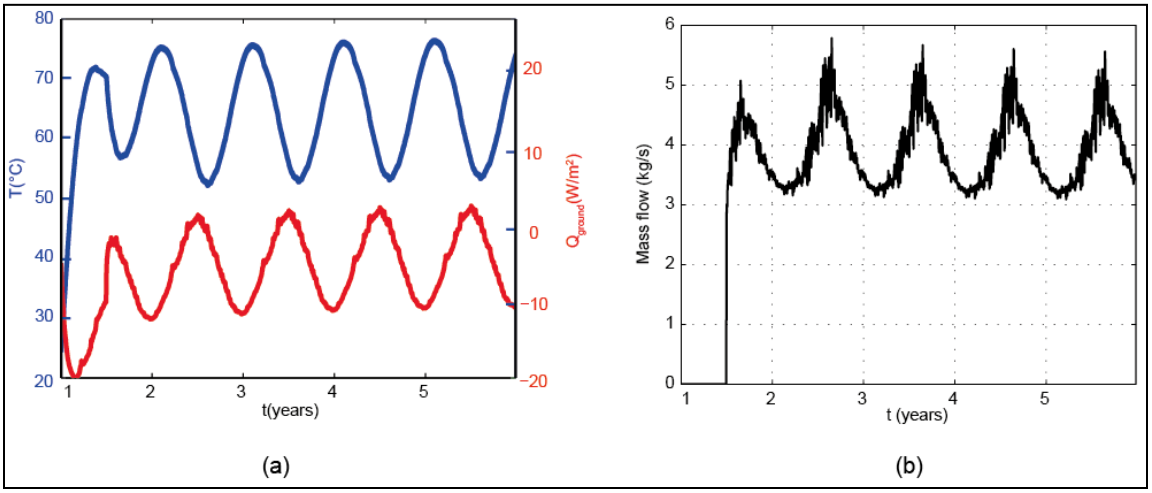

Figure 3-4: Simulations of the baseline scenario: (a) thermal evolution in the LCZ and ground heat losses; (b) mass flow rate evolution.

3.4.2 Alternative scenario: SGSP with insulation layer

When the insulation layer is added, the average temperature in the LCZ increases because the heat losses to the ground are reduced, as shown in Figure 2-5. When the thickness of the insulation layer increases, the stored heat in the ground decreases and the total heat storage volume is reduced to the LCZ volume. As the heat storage volume is smaller, the thermal evolution of the LCZ is more sensible to atmospheric changes, which implies more variability in temperatures through the year (Figure 2-6(a)). For example, when the insulation layer has a thickness of 10 cm, the LCZ temperatures are 2.7% higher than those observed in the baseline scenario during the summer months, but 2.5% lower during the winter months. For the present study, the addition of an insulation layer of polystyrene is not economically convenient, as the investment costs are higher than the benefits of reducing the pumping costs. Even more, thin insulation layers (≤ 10 cm) do not bring benefits in reducing the pumping cost, as the average friction losses in the pipes –for extracting the same amount of heat– are higher than those of the baseline scenario. From equations (2.7) and (2.8), an implicit relationship between the temperature in the LCZ and the mass flow rate required to satisfy the heat extraction rate can be inferred: the mass flow rate increases exponentially as the temperature in the LCZ decreases (Figure 2-6(b)). Therefore, even if the average temperatures are higher when an insulation layer is used, the annual pumping operation can still cost more than the baseline scenario as the additional pumping cost of lower temperatures during winter can be higher than the benefits of having higher temperatures in summer.

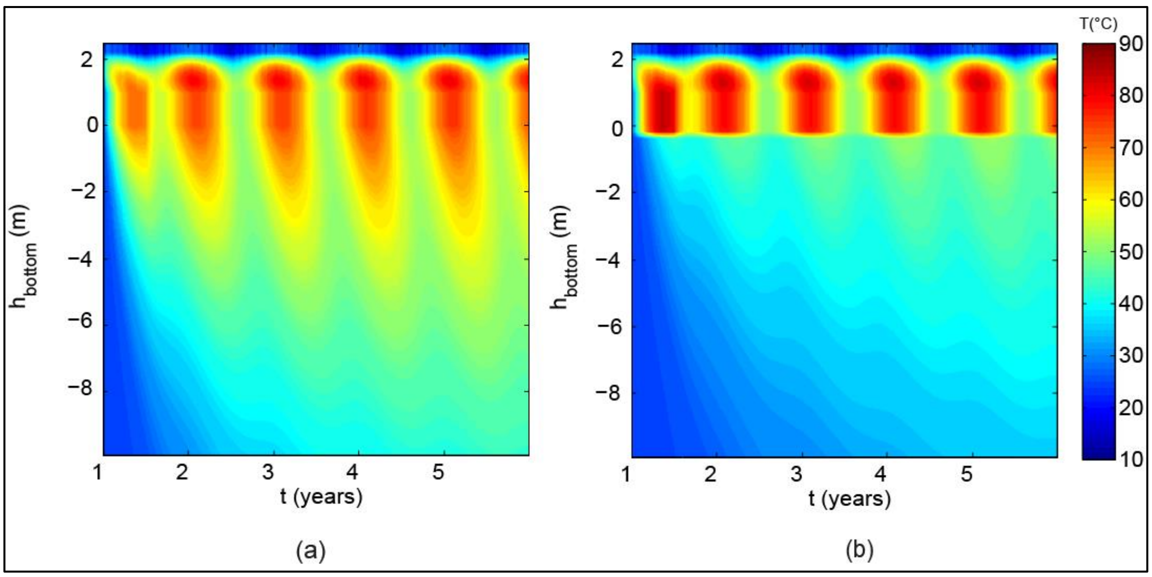

Figure 3-5: Thermal evolution of the SGSP and the ground beneath it: (a) without insulation; (b) with a 20 cm insulation layer.

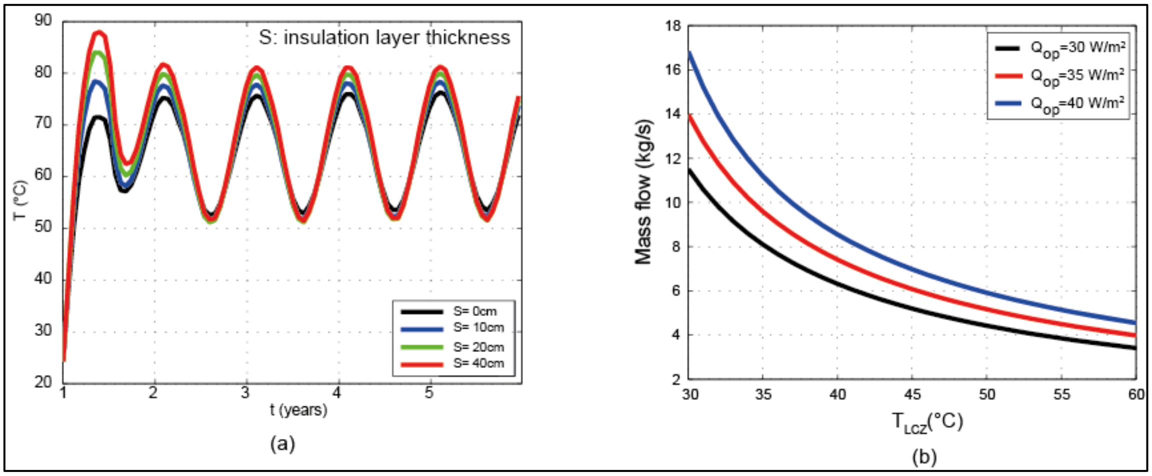

Figure 3-6: (a) Thermal evolution of the LCZ with different insulation layer's thickness. (b) Exponential relation between the mass flow rate and the LCZ temperatures.

3.4.3 Ground thermal properties and water table depth

Figure 2-7(a) shows a sensitivity analysis made on the ground's thermal conductivity, specific capacity and on the water table depth (WTD). The three variables are varied in ±75% to study their impact on the LCZ average temperatures. To quantify a variable's impact, the rate of change is defined as it follows:

$$Rate\ of\ change = \frac{\Delta T_{LCZ,avg}(\%)}{\Delta Variable\ (\%)} \tag{2.12}$$

Results show that the most influent variables are the ground thermal conductivity and the WTD. Thermal conductivity has a linear relation with the LCZ temperature, with an almost constant rate of change of -0.04, which means that for every 1% increment in thermal conductivity, the LCZ average temperature decreases in 0.04%. On the other hand, the relation between the LCZ temperature and the WTD is logarithmic. For WTDs shallower than 9 m, the rate of change is over 0.78 and the ground is not able to store more heat, as the heat is lost to the water table. When the water table is at 9 m depth, ground heat losses are 121% higher than those observed in the baseline scenario and no heat is recovered during the winter period: all the heat is lost to the water table (Figure 2-7(b)). Additionally, when the WTD is deeper than 21 m, the rate of change is lower than 0.004, which means that heat losses from the LCZ to the water table are negligible.

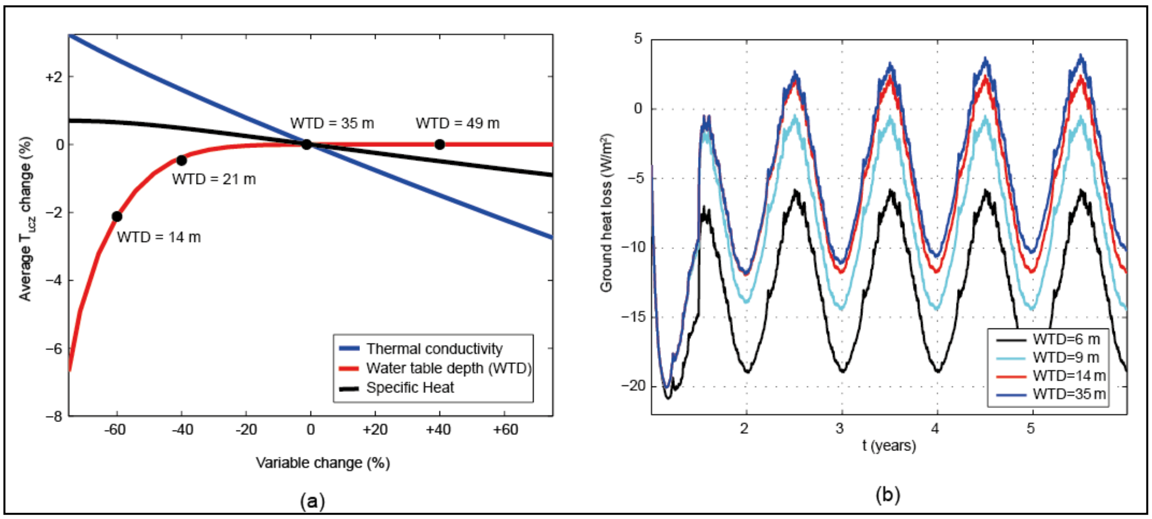

Figure 3-7: (a) Sensitivity analysis: thermal conductivity, WTD and specific heat. (b) Ground heat losses for different WTDs.

3.5 Conclusions

Heat storage in the ground beneath a solar pond can have a positive impact in the performance of a solar pond when heat is extracted at a constant rate from the LCZ. When quasi-steady state is reached, 25.5% of the heat lost to the ground is recovered back to the pond in the winter period, and temperatures in the LCZ are more stable throughout the year (compared to the scenarios were an insulation layer was used). The addition of a polystyrene insulation layer is not economically convenient, as the investment costs of it are higher than the benefits of lowering the pumping costs. A sensitivity analysis showed that when the WTD is shallower than 9 m, the ground does not act as a heat storage unit as all the heat is lost towards the groundwater.

4 CONCLUSIONS AND PERSPECTIVES

In this study a simplified one-dimensional transient model to predict the temperatures distribution in a SGSP and the ground beneath it was developed. The model was calibrated and validated with an experimental SGSP heated with high-intensity discharge lamps. The agreement between experimental and modeled temperatures was very good, with a RMSE's of 1.35 and 1.13 °C in the UCZ and LCZ, respectively. Further, it was demonstrated that the model also correctly predicted the temperature evolution of three different SGSP exposed to natural solar radiation.

The use of multiple layers to represent the ground beneath a SGSP showed to be a good feature to incorporate in unsteady SGSP's models, as they allow the simulation of the ground heat storage, which can have a positive impact in the performance of a solar pond.

According to the modeled results in Chapter 2, when heat is extracted at a constant rate from the LCZ and the quasi-steady state is reached, 25.5% of the heat lost to the ground can be recovered back to the pond in the winter period when no insulation was used, and temperatures in the LCZ are more stable throughout the year (compared to the scenarios were an insulation layer was used). Nevertheless, the sensitivity analysis showed that when the water table depth was shallower than 9 m, the ground did not act as a heat storage unit as all the heat was lost towards the groundwater.

The model developed in this investigation is flexible and can be used for experimental or large-scale SGSP designs. Further, these designs should include a study of the ground thermal properties and the groundwater table depth, and based on this information evaluate if the ground heat storage could improve the SGSPs operation.

Future work should consider validating the model with SGSPs where heat is extracted and where detailed information of the ground's temperature distribution is available.

REFERENCES

Abdullah, A.A., Lindsay, K.A. and AbdelGawad A.F. (2016). Construction of sustainable heat extraction system and a new scheme of temperature measurement in an experimental solar pond for performance enhancement. *Solar Energy*, 130, 10-24.

Adams, E., Cosler, D. and Helfrich, K. (1990). Evaporation from heated water bodies - predicting combined forced plus free-convection. *Water Resour. Res*., 26(3), 425–435.

Ali, H.M. (1986). Mathematical modelling of salt gradient solar pond performance. *Energy Research*, 10, 377-384.

Bernad, F., Casas, S., Gibert, O., Akbarzadeh, A., Cortina, J.L. and Valderrama C. (2013). Salinity gradient solar pond: Validation and simulation model. *Solar Energy*, 98, 366-374.

Bronicki, L.Y. (2013). Solar Ponds, *Earth Systems and Environmental Sciences*.

Busquets, E., Kumar, V., Motta, J., Chacon, R. and Lu, H. (2012). Thermal analysis and measurement of a solar pond prototype to study the non-convective zone salt gradient stability. *Solar Energy*, 86, 1366–1377.

Chen S.X. (2008). Thermal conductivity of sands. *Heat and Mass Transfer*, 44, 1241-1246.

Date, A., Yaakob, Y., Date, A., Krishnapillai, S. and Akbarzadeh, A. (2013). Heat extraction from Non-Convective and Lower Convective Zones of the solar pond: A transient study. *Solar Energy*, 97, 517-528.

Dirección General de Aguas (2004). Cuenca del río Copiapó: diagnóstico y clasificación de los cursos y cuerpos de agua según objetivos de calidad.

El-Sebaii, A.A., Ramadan, M.R.I., Aboul-Enein, S. and Khallaf, A.M. (2011). History of the solar ponds: A review study. *Renewable and Sustainable Energy Reviews*, 15, 3319-3325.

Garrido, F. and Vergara, J. (2013). Design of solar pond for water preheating used in copper cathodes washing at a mining operation at Sierra Gorda, Chile. *Journal of Renewable and Sustainable Energy*, 5, 043103.

Garrido, F., Soto, R., Vergara, J., Walczak, M., Kanehl, P., Nel, R. and García, J. (2012). Solar pond technology for large-scale heat processing in a chilean mine. *Journal of Renewable and Sustainable Energy*, 4, 053115.

Hawas, M.M. and Elasfouri, A.S. (1985). Performance of a salt-gradient solar pond for power production. *Energy Conversion Management*, 25(3), 323-330.

Henderson-Sellers, B. (1986). Calculating the surface energy balance for lake and reservoir modeling: a review. *Rev. Geophys*., 24, 625–649.

Hilgersom, K., Suárez, F., Zijlema, M., Hausner, M.B., Tyler, S. and Van de Giesen, N. Heat and salt transport near the sloping edge of a solar pond: a two-dimensional numerical study. *Under review in the International Journal of Heat and Mass Transfer.*

Hull, J.R., Nielsen C.E. and Golding P. (1989). Salinity-gradient solar ponds. CRC Press, Boca Raton, Florida.

International Standard EN-ISO (2007). Building materials and products - Hygrothermal properties - Tabulated design values and procedures for determining declared and design thermal values.

Jaefarzadeh, M.R. (2006). Heat extraction from a salinity-gradient solar pond using in pond heat exchanger. *Applied Thermal Engineering*, 26, 1858-1865.

Kannan, N. and Vakeesan, D. (2016). Solar energy for future world: a review. *Renewable and Sustainable Energy Review,* 62, 1092– 1104.

Kauffmann, D.W. (1960). Sodium Chloride, Reinhold, New York.

Kurt, H., Ozkaymak, M. and Binark, A.K. (2006). Experimental and numerical analysis of sodium-carbonate salt gradient solar-pond performance under simulated solar-radiation. *Applied Energy*, 83, 324-342.

Kurt, H., Halici, F. and Binark A.K. (2000). Solar pond conception – experimental and theoretical studies. *Energy Conversion & Management*, 41, 939-951.

Leblanc, J., Akbarzadeh, A., Andrews, J., Lu, H. and Golding, P. (2011). Heat extraction methods from salinity gradient solar ponds and introduction of a novel system of heat extraction for improved efficiency. *Solar Energy,* 85, 3103-3142.

Losordo, T. and Piedrahita, R. (1991). Modelling temperature-variation and thermal stratification in shallow aquaculture ponds. *Ecol. Model*., 54(3–4), 189–226.

Lu, H., Walton, J.C. and Swift, A. (2001). Desalination coupled with salinity-gradient solar ponds. *Desalination,* 136, 13-23.

Panwar, N., Kaushik, S. and Kothari, S. (2011). Role of renewable energy sources in environmental protection: a review. *Renewable and Sustainable Energy Review*, 15(3), 1513– 1524.

Prasad, R. and Rao, D.P. (1993). Feasibility studies on the enhancement of energy storage in the ground beneath solar ponds. *Solar Energy*, 50, 135-144.

Rabl, A. and Nielsen, C. (1975). Solar ponds for space heating. *Solar Energy*, 17, 1–12.

Ruskowitz, J.A., Suárez, F., Tyler, S.W. and Childress, A.E. (2014). Evaporation suppression and solar energy collection in a salt-gradient solar pond. *Solar Energy*, 99, 36-46.

Saleh, A., Qudeiri, J.A. and Al-Nimr, M.A. (2011). Performance investigation of a salt gradient solar pond coupled with desalination facility near the Dead Sea. *Energy*, 36, 922-931.

Sayer A.H., Al-Hussaini and Campbell A.N. (2016). New theoretical modeling of heat transfer in solar ponds. *Solar Energy*, 125, 207-218.

Sezai, I. and Tasdemiroglu, E. (1995). Effect of bottom reflectivity and ground heat losses for solar ponds. *Solar Energy*, 55, 311-319.

Singh, R., Tundee, S. and Akbarzadeh, A. (2011). Electric power generation from solar pond using thermophyson and thermoelectric modules. *Solar Energy*, 85, 371-378.

Singh, T.P., Singh, A.K. and Kaushika, N.D. (1994). Investigations of thermohydrodynamic instabilities and ground storage in a solar pond by simulation model. *Heat Recovery Systems & CHP*, 14(4), 401-407.

Soto M.C. (2010). Hidrogeología e hidroquímica de aguas subterráneas en el distrito de Inca de Oro, Región de Atacama: procesos de interacción agua-roca y dispersion geoquímica. *M.Sc. Thesis*, University of Chile, Santiago, Chile.

Styris, D.L. and Harling, O.K. (1976). The non convecting solar pond applied to building and process heating. *Solar Energy*, 18, 245-251.

Suárez F., Urtubia, R. (2016). Tackling the water-energy nexus: membrane distillation driven by solar ponds, *Clean Technologies and Environmental Policy*.

Suárez, F., Ruskowitz, J.A., Tyler, S.W. and Childress, A.E. (2015). Renewable water: direct contact membrane distillation coupled with solar ponds. *Applied Energy*, 158, 532-539.

Suárez, F., Ruskowitz, J., Childress, A.E. and Tyler, S.W. (2014a). Understanding the expected performance of large-scale solar ponds from laboratory-scale observations and numerical modeling. *Applied Energy*, 117, 1-10.

Suárez, F., Muñoz, J.F., Fernández, B., Dorsaz, J., Hunter, C.K., Karavitis, C.A. and Gironás, J. (2014). Integrated water resource management and energy requirements for water supply in the Copiapó river basin, Chile. *Water*, 6, 2590-2613.

Suárez, F., Aravena, J.E., Hausner, M.B., Childress, A.E. and Tyler, S.W. (2011). Assessment of a vertical high-resolution distributed-temperature-sensing system in a shallow thermohaline environment. *Hydrology and Earth System Sciences*, 15, 1081-1093.

Suárez, F., Tyler, S.W. and Childress, A.E. (2010a). A theoretical study of a direct contact membrane distillation system coupled to a salt-gradient solar pond for terminal lakes reclamation. *Water Research*, 44, 4600–4615.

Suárez, F., Tyler, S.W. and Childress, A.E. (2010b) A fully coupled, transient double-diffusive convective model for salt-gradient solar ponds. *International Journal of Heat and Mass Transfer*, 53, 1718–1730.

Tundee, S., Terdtoon, P., Saculchangsatjatai, P., Singh, R and Akbarzadeh, A. (2010). Heat extraction from salinity-gradient solar ponds using heat pipe heat exchangers. *Solar Energy*, 84, 1706-1716.

Valderrama, C., Gibert, O., Arcal, J., Solano, P., Akbarzadeh, A., Larrotcha, E. and Cortina, J.L. (2011). Solar energy storage by salinity gradient solar pond: Pilot plant construction and gradient control. *Desalination*, 279, 445-450.

Vogelesang, H. (2008). An introduction to energy consumption in pumps, WorldPumps.

Wang Y.F. and Akbarzadeh A. (1982). A study on the transient behavior of solar ponds. *Energy*, 7(12), 1005-1017.

Weinberger, H. (1964). The physics of the solar pond. *Solar Energy*, 8, 45-56.

Yunus, A.C. and Cimbala, J.M. (2010). Fluid Mechanics: Fundamentals and Applications, McGraw-Hill.

Zhang, Z.M. and Wang, Y.F. (1990). A study on the thermal storage of ground beneath solar ponds by computer simulation. *Solar Energy*, 44, 243-248.